8-2011

The Development and Implementation of an Anthropomorphic Head Phantom for the Assessment of Proton Therapy Treatment Procedures

Paige A. Summers

DEVELOPMENT AND IMPLEMENTATION OF AN ANTHROPOMORPHIC HEAD PHANTOM FOR THE ASSESSMENT OF PROTON THERAPY TREATMENT PROCEDURES

by

Paige Alexandra Summers, B.S.

APPROVED:

_____
Supervisory Professor – Geoffrey Ibbott, Ph.D.

_____
[David Followill, Ph.D.]

_____
[Falk Pönisch, Ph.D.]

_____
[Narayan Sahoo, Ph.D.]

_____
[Susan Tucker, Ph.D.]

(All signatures must be in black ink.)

APPROVED:

_____
Dean, The University of Texas
Graduate School of Biomedical Sciences at Houston

DEVELOPMENT AND IMPLEMENTATION OF AN ANTHROPOMORPHIC HEAD PHANTOM FOR THE ASSESSMENT OF PROTON THERAPY TREATMENT PROCEDURES

A

THESIS

Presented to the Faculty of
The University of Texas
Health Science Center at Houston
and
The University of Texas
M. D. Anderson Cancer Center
Graduate School of Biomedical Sciences
in Partial Fulfillment

of the Requirements

for the Degree of

MASTER OF SCIENCE

by

Paige Alexandra Summers, B.S.
Houston, Texas

August 2011

Dedication

To mama,
because this was always the plan.

Acknowledgements

I would like to acknowledge and thank my Supervisory committee, chair Geoffrey Ibbott, Ph.D., David Followill, Ph.D., Narayan Sahoo, Ph.D., Falk Pönisch, Ph.D., and Susan Tucker, Ph.D. for their insight and support.

I would also like to thank X. Ronald Zhu, Ph.D. and Michael Gillin, Ph.D for their help with proton therapy delivery, John Costales, our phantom engineer, David Lege, our proton dosimetrist, Beverly Riley, Jaques Bluett, Jason Stafford, Ph.D, our MR expert, and Shane, our CT tech.

Thanks, also, to Ryan Grant, Tony Blatnica, and Jacqueline Tonigan for their help with design and irradiations.

Lastly, thank you to my family and friends for their love and support throughout my academic adventures.

Development and Implementation of an Anthropomorphic Head Phantom for the Assessment of Proton Therapy Treatment Procedures

Publication No._____

Paige A. Summers, B.S.

Supervisory Professor: Geoffrey S. Ibbott, Ph.D.

Proton therapy has become an increasingly more common method of radiation therapy, with the dose sparing to distal tissue making it an appealing option, particularly for treatment of brain tumors. This study sought to develop a head phantom for the Radiological Physics Center (RPC), the first to be used for credentialing of institutions wishing to participate in clinical trials involving brain tumor treatment of proton therapy. It was hypothesized that a head phantom could be created for the evaluation of proton therapy treatment procedures (treatment simulation, planning, and delivery) to assure agreement between the measured dose and calculated dose within ±5%/3mm with a reproducibility of ±3%. The relative stopping power (RSP) and Hounsfield Units (HU) were measured for potential phantom materials and a human skull was cast in tissue-equivalent Alderson material (RLSP 1.00, HU 16) with anatomical airways and a cylindrical hole for imaging and dosimetry inserts drilled into the phantom material. Two treatment plans, proton passive scattering and proton spot scanning, were created. Thermoluminescent dosimeters (TLDs) and film were loaded into the phantom dosimetry insert. Each treatment plan was delivered three separate times. Each treatment plan passed our 5%/3mm criteria, with a reproducibility of ±3%. The hypothesis was accepted and the phantom was found to be suitable for remote audits of proton therapy treatment facilities.

Table of Contents

Table of Illustrations

List of Tables

Chapter 1

1 Introduction and Background

1.1 Statement of Problem

1.1.1 General Problem Area

With about 2500 medical facilities treating over a million cancer patients with radiation therapy modalities in the United States each year, there is a need to assure that the treatment a patient gets in one area of the country is of the highest quality and not significantly different than what one would expect to receive in another region (1). Similarly, if institutions are participating in National Cancer Institute (NCI) funded clinical trials involving radiation therapy trials, there needs to be some way of assuring the specific Study Groups sponsoring the trials that each site is qualified and capable of following the requirements of trial protocols. With over 1800 institutions participating in more than 100 clinical trials involving radiation therapy, there are a significant number of patients affected by the quality of radiation treatment. Treatment facilities are already encouraged to carry out their own quality assurance (QA) programs, per recommendations published by the International Commission on Radiation Units and Measurements (ICRU) and contained in the American Association of Physics in Medicine Task Group reports (AAPM TG reports), but there are currently very few groups that assure excellence and consistency between independent radiation treatment centers across North America.

The Radiological Physics Center (RPC), based at MD Anderson Cancer Center in Houston, TX, is a QA group funded by the NCI who is charged with monitoring medical institutions participating in clinical trials. The RPC was created with the goal of assuring the NCI and cooperative clinical trial Study Groups that radiation dose delivered to trial patients are "clinically comparable and consistent" (2). The RPC, unlike other QA groups funded by the NCI who only monitor a fraction of the trial participants, monitors all participating institutions (nearly 1850 sites) that participate in all cooperative group clinical trials funded by the NCI. The RPC uses both onsite audit visits and remote mailable dosimetric audit systems to assess the efficacy of each institution's radiation therapy procedures. The remote audit mailable program includes: (1) verification of an

institution's machine output using thermoluminescent detectors (TLDs) or optically stimulated luminescent detectors, (2) Verification of the patient treatment records sent to the RPC for review and (3) Credentialing institutions through the use of the RPC's anthropomorphic QA phantoms that evaluate an institution's ability to deliver a specific treatment end to end, i.e. from imaging to planning to setup to dose delivery. The RPC has numerous phantoms for photon therapies, including SRS head, head & neck, spine, thoracic/lung, pelvic/prostate, and liver phantoms, but very few for proton therapy.

1.1.2 Specific Problem

Radiation Oncology therapy as given today is highly dependent on advances in technology and computerization of treatments. One of the advanced technologies used to treat patients is proton therapy. Although proton therapy has been around for some time, recent advances in delivery techniques such as scanning beams and intensity modulated proton therapy, have increased its popularity in the Radiation Oncology community, particularly in the United States. According to the National Association for Proton Therapy (3), there are currently nine proton centers treating patients, four more under construction, and another 8-10 in the planning stages whereas only 5 years ago there were only 3 centers treating patients. As proton therapy becomes more widely used to treat certain types of patients, this form of therapy will be included as a radiation delivery option in NCI funded clinical trials. As proton facilities look to enroll patients in clinical trials, there is a need to evaluate each institution's ability to provide accurate, precise and consistent treatments.

The NCI wants the scientific integrity of its clinical trials to be flawless and as such has funded several quality assurance groups to assist the Study Groups and to monitor those institutions participating in clinical trials. One monitoring group, the Quality Assurance Review Center (QARC), provides treatment record quality assurance and data management for six NCI cooperative groups(4). Because of QARC's relationship with the Children's Oncology Group (COG), it has been involved in providing some proton therapy QA through the use of a questionnaire and proton therapy benchmark case. The questionnaire allows QARC to assess the institution's resources, personnel and experience, while the benchmark case gives them confidence that the

institution can properly generate a treatment plan given guidance from a protocol (4). While QARC and other monitoring bodies review records and monitor safety protocol and violations, the RPC is the only group that oversees the quality of radiation therapy.

As such, the RPC is the quality assurance group best suited to develop a credentialing process for the evaluation of proton therapy. Generally the RPC credentialing procedure includes a site visit to the institution of interest where measurements are taken using phantoms and dosimeters to assess the quality of radiation therapy being delivered at the facility. With the introduction of proton therapy in clinical trials, the RPC adapted two phantoms for the use in proton credentialing: a pelvis and lung phantom (5, 6). The lung phantom had been modified with the use of balsa wood as a lung-equivalent material, due to the similarities between balsa wood's stopping power and CT number in relation to the lungs' correlating properties. The pelvic phantom was similarly modified by changing the target and critical structure phantom materials to more closely mimic corresponding anatomy based on stopping power and CT numbers. The phantoms test the proton systems ability to deliver a conformal dose to a target, and in the case of the pelvis phantom, avoid dose to surrounding critical structures. While dosimetric methods and QA phantoms for testing radiation therapy facilities have adapted to new developments in treatment modalities including proton therapy, the RPC does not at this time have a mailable anthropomorphic head & neck phantom available to test proton therapy treatment.

1.1.3 Importance of Topic

Quality control of radiation therapy is of utmost importance in assuring proper treatment of patients as well as the safety of patients and personnel in the radiation oncology field. However, the role of quality control has taken on new importance with the lay press drawing increasing attention to radiation therapy incidents and medical errors. A series of articles published in The New York Times in the Winter of 2010 exposed malpractice and radiation therapy errors, some of which led to serious complications as well as fatalities of patients who had been mistreated (7, 8). From there, the media has continued to draw attention to dangers of radiation oncology and there has

been heightened skepticism of radiation therapy practices both by media sources and the general public.

As delineated in one of the articles, new modalities are often accepted for use in treating patients with little attention to how safety and quality assurance procedures may have to be changed based on the newly employed advanced technology (7). Recognizing that proton therapy requires distinctive QA procedures, the ICRU recommends quality assurance checks for proton therapy that cover the treatment delivery system, patient positioning and immobilization, and treatment planning (9). However, most centers using proton therapy generally develop their own quality assurance practices specific to their unique setup (e.g. different tests for passively scattered beams v. scanning beams, etc.) following the basic principles laid out in the ICRU recommendations. Due to the variety of QA programs and measurement techniques throughout the existing proton therapy institutions, an independent evaluation of the accuracy of treatment delivery at each center is needed if they are to participate in clinical trials. One technique to perform this independent evaluation is through the use of one of the RPC's anthropomorphic QA phantoms built especially for proton therapy. Once the QA phantom is developed by the RPC, it will be beneficial in ensuring nationwide treatment conformity, as well as compliance of the radiation therapy centers participating in research protocols.

Quality assurance for proton therapy is just as, if not more, important as quality assurance for other radiation therapy modalities. While the behavior of the proton Bragg peak makes protons great for killing cancer cells, it also has a great potential to damage healthy tissue if the range of the proton beam is miscalculated and regular tissue is accidentally irradiated. Proton therapy, as mentioned in the introduction, has unique requirements for quality assurance because different facilities have different machines and equipment. In regards to beam calibration, it is recommended by the ICRU, and required by the NCI for centers participating in cooperative group trials, that each proton beam be calibrated according to TRS 398. This protocol walks each center through the determination of the absorbed dose to water for the proton beam using a parallel plate or cylindrical ion chamber, depending on the residual range (10).

Regular quality assurance procedures, however, have looser guidelines, as each facility has set up their own method of checking the accuracy and precision of their

proton therapy treatment system. The ICRU has summarized some suggested quality assurance procedures for both passive and scanning beam systems, as collected from site-specific QA publications. These recommendations include daily checks of the beam aperture alignment, room lasers, safety interlocks, patient communication systems and patient positioning, depth dose and lateral beam profiles, monitor units and dose monitors, and individual patient treatment setup, with additional checks required for scanning beam systems, including dose rate, monitor ratios, beam position monitors, depth dose curves in water, and calibration of the primary dose monitor (9). Weekly checks include patient positioning and imaging modalities, beam-line apparatus, breath cycle equipment, and verification of one patient dose in water (to be examined in three dimensions for scanning beams) (9). Semi-annual, annual, or scheduled checks include calibration of CT scanner Hounsfield units, x-ray alignment, tests of all therapy equipment, and calibration of the primary dose monitor, and beam characteristics for scanning beams (9). While most facilities follow these general practices, there is room for variation as each center employs equipment developed by different manufacturers.

While it is not possible at this time to get every proton center to follow the exact same quality assurance protocol, which might ensure consistency in performance across centers, it is possible to review each center's performance to ensure that their individualized QA procedures are working. Beyond a uniform initial beam calibration, the NCI has set forth additional guidelines for proton therapy centers looking to participate in clinical trials. The NCI requires that these centers go through a credentialing process with the RPC for the cooperative group running the trial. The centers undergo a credentialing process through the RPC that includes several steps. These steps include completion of a questionnaire, annual monitoring of the reference proton beam outputs with the RPC's TLD audit and dosimetry onsite visits that include dosimetry measurements, review of QA procedures and a phantom irradiation. Part of the RPC's visit is to assure accuracy of the proton center's Hounsfield to Stopping Power conversion, treatment planning algorithm, and patient specific immobilization system (11). There are a handful of other guidelines put forth by the NCI as well: a radiation oncologist must be involved in the implementation of the clinical trial at each institution, all doses must be expressed in terms of Cobalt Gray Equivalent (CGE) using an RBE of

1.1, and while GTV and CTV for treatment planning must be the same as it would for photon protocol, the PTV created for each lesion should take into account site-specific beam characteristics, such as lateral beam scattering and range uncertainties (11).

1.2 Hypothesis

With the current relevance and importance of proton therapy quality assurance, this project is particularly timely. The hypothesis of this project is as follows: An anthropomorphic head phantom can be created to evaluate proton therapy treatment procedures (patient simulation, treatment planning, and treatment delivery) to assure agreement between the measured dose and calculated dose within ±5%/3mm with a reproducibility of ±3%. With this goal in mind, the specific aims of this project are:

1. Select a suitable head phantom design, evaluate tissue equivalent materials for corresponding relevant patient anatomy and build the head phantom.
2. Image the head phantom, create two clinically relevant proton therapy treatment plans using the passive scattered and spot scanning proton beams, and irradiate the phantom multiple times with each treatment plan.
3. Measure the delivered dose distribution and the dose to specific points inside the irradiated phantom.
4. Compare the measured and calculated point doses and 2D dose distributions to determine deviations and precision.

1.3 Research Approach

In order to achieve the specific aims of the project, the following methodology will be employed:

1. The stopping power and Hounsfield Units (HU) will be determined for the phantom materials and compared to known stopping powers and Hounsfield Units of corresponding human anatomy used for proton therapy.
2. The phantom will be imaged with MRI and this image will be fused with a CT image set for target delineation and dose distribution calculations. Two treatment plans will be designed using these images in the Eclipse proton planning system,

according to the department's standards for both the passive scattering and spot scanning systems. The plans will be developed based on typical clinical constraints used for designing treatment plans for brain cancer targets at the Proton Therapy Center – Houston (PTC-H) and a radiation oncologist will review and approve the final plans.

3. Radiochromic film and TLD capsules will be placed inside the phantom's cylindrical dosimetry insert and the phantom will be irradiated according to the treatment plan. Each plan will be delivered a minimum of three separate times to assess reproducibility of the phantom audit system.

4. The 2D dose distributions and absolute point doses determined from the film and TLD will be compared with the calculated values of point doses, dose profiles and planar dose distributions from the treatment planning system to determine the agreement and reproducibility.

1.4 Limitations

There are two primary challenges in the development of a head phantom that can be used to audit proton therapy for targets in the head. The first challenge is the creation of a phantom that can be imaged appropriately. The latest Radiation Therapy Oncology Group (RTOG) protocol, RTOG 0539, on the treatment of Meningioma requires that the head be imaged using MRI for the purposes of lesion delineation, and then fused with a CT image for dose calculation purposes (12). Anthropomorphic phantoms, however, are not usually imaged with MRI since the solid materials that comprise the phantoms are not well delineated with most MR imaging sequences. While it would be easy enough to mail out this phantom with instructions to take a CT image instead of MR, it is desired that the auditing process mirror typical treatment protocol and therefore the audit should encompass the imaging component of the treatment delivery process. The second challenge is determining what materials are to be used in the construction of the phantom such that they are tissue equivalent based on proton interactions. The tissue substitute materials used with photons do not necessarily meet the requirements to be substitute materials for protons. Based on these two challenges, the difficulty comes in finding phantom materials that are solid, tissue equivalent based on proton interactions, and show

up on an MRI. In addition, it is desired that the tumor be visible in the MR image, but not easily distinguishable on a CT image.

The RTOG 0539 protocol also recommends head immobilization tactics such as cast immobilization, modified stereotactic frame, or a camera-based localization setup (12). These requirements are hard to meet due to the structure and solid nature of the phantom, so special considerations have to be made for phantom immobilization. The protocol also requires that weekly portal imaging be used for the initial treatment setup, as well as periodically throughout the course of treatment (film or EPID). While the periodic imaging cannot be integrated into phantom irradiations, the initial treatment setup will utilize on-board imaging.

1.5 Literature Review

1.5.1 Proton Background

Proton therapy has long been of interest in the medical community due to the behavior of protons in a medium. The existence of protons was suggested by Rutherford in 1919 and the first particle accelerator was developed in 1930; 16 years later, it was suggested that protons could be used for treatment of cancer (13, 14). What is exciting about proton therapy is that protons, basic subatomic charged particles, follow the theory of the continuous slowing down approximation, and the rate of energy loss of a proton particle is found to be inversely proportional to the square of its velocity (15). As a proton collides with other particles in a medium and experiences a decrease in velocity, the energy loss is greatly increased causing a characteristic energy deposition known as the Bragg peak. When beams of different energies are superimposed to create a spread out Bragg peak (SOBP) in depth, the area of high energy deposition can be used to treat a tumor of finite thickness as seen in Figure 1.1. In addition to the high dose region of an SOBP, protons exhibit relatively low energy deposition on the proximal side of the peak, and extremely low amounts of energy deposited on the distal side of the peak (13). This is an advantage (in theory) of protons over more conventional therapeutic modalities such as electrons, which have a higher relative entrance dose for both skin and proximal target tissues, and photons, which exhibit a greater distal dose, as shown in Figure 1.1.

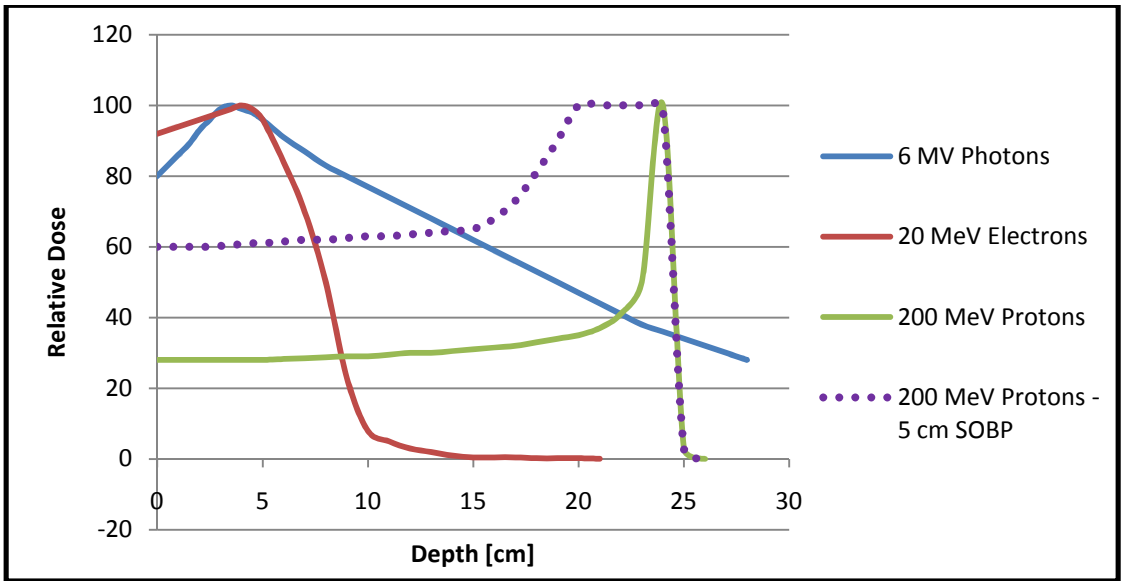

Figure 1.1 Relative Depth-Dose curves of 6 MV photons, 20 MeV electrons, pristine 200 MeV protons, and a spread-out 200 MeV proton beam

The steep energy drop-off on the distal side of the proton SOBP means that the dose prescribed to the lesion can deliver a highly conformal dose while sparing the healthy tissue, or perhaps an organ at risk, especially that is located distal to the range of the proton beam, indicating a possible advantage over photon therapy.

When a proton interacts with matter, it loses small portions of its energy due to electromagnetic interactions with atomic electrons (15). The quantification of a proton's energy loss over a finite thickness of absorbing material is defined by the term mass stopping power. The mass stopping power can be expressed as below (16):

$$\frac{S(E)}{\rho} = \frac{4\pi r^2 mc^2 Z z^2 L(\beta)}{\beta^2 uA} \qquad \textbf{Equation 1.1}$$

$E)\rho = 4\pi r^2 mc^2 Z z^2 L(\beta)\beta^2 uA$ Equation 1.1 takes into account the radius of the electron orbit (r), the rest energy of an electron (mc^2), the atomic number of the stopping material (Z), the charge of the proton (z), the ratio of the proton's velocity to the speed of light (β^2), the atomic mass unit (u), the atomic mass of the stopping material (A), and the stopping number ($L(\beta)$). The mass stopping power value takes into account the mean excitation energy of atoms in the stopping material, the effect of atomic shells, and the density-effect, or the effective reduction of stopping power due to the proton's projectile polarization (16).

1.5.2 Biological Impact of Protons

In addition to the advantages that protons present due to their characteristic range, protons are thought to have a greater biological impact than other therapeutic particles, which can be more effective in causing damage in cancer cells. This higher biological impact is caused by an increase in ionization along the path of the particle. Relative biological effectiveness (RBE) is expressed as:

$$\boldsymbol{RBE = \frac{Dose_{ref}}{Dose}} \qquad \textbf{Equation 1.2}$$

In $\boldsymbol{RBE = \frac{Dose_{ref}}{Dose}}$ Equation 1.2, *Dose* and $Dose_{ref}$ are the doses required to cause the same biological effect. The reference dose, $Dose_{ref}$, is based upon either ^{60}Co or 250 kVp photons (17). When using such a reference dose, an RBE of 1.1 is generally accepted and used for protons (11, 18, 19). This means that protons themselves have a higher RBE than conventional treatment with photons and electrons. In addition, nuclear reactions with protons cause secondary particles (such as neutrons) that have greater RBE, and can be more effective in killing the cells that make up cancerous lesions (15).

When speaking of dose delivered by protons, the RBE is usually taken into account and the dose is expressed in terms of Cobalt Gray Equivalent (CGE). The equation for CGE for protons is listed in $\boldsymbol{CGE = 1.1 * Dose_{proton}}$ Equation 1.3 (20, 21):

$$\boldsymbol{CGE = 1.1 * Dose_{proton}} \qquad \textbf{Equation 1.3}$$

The above equation gives a value for dose, expressed in units of Gray (Gy), that is comparable to photon or electron dose that have an RBE equal to 1.0. For uniformity and clarity purposes, the NCI requires that radiation therapy groups participating in clinical trials use CGE for dose information and prescription (11). It should be noted, however, that many proton clinics are using the unit of Gy_{RBE} in reference to RBE dose.

1.5.3 Proton Therapy Beam Development

Protons used for therapy purposes are generally

The two most basic categories of proton

1.5.3.1 Passive Scattering

When the accelerated protons reach the gantry,

The SOBP is created by beam range

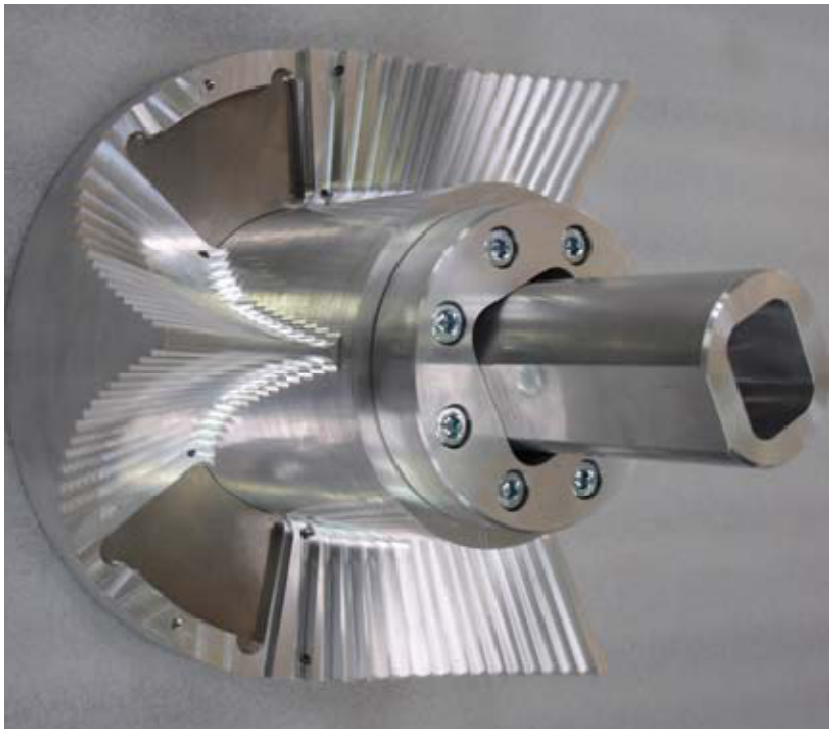

Figure 1.2. Range Modulation Wheel (5)

Figure 1.3. 160 (ID84) and 140 (ID85) MeV RMWs used at the PTC-H

The range of the protons can also be varied by inserting additional absorbers in the beam path, as well as by changing the energy of the beam (18). At the PTC-H, range shifters are introduced after the scatterers and RMW to shift the beam range in increments of 1 mm.

The passive scatter beam is also shaped by apertures and compensators (see Section 2.3.2.1 for images). The apertures are thick sheets of brass that are shaped according to the outline of the target and placed on the outer edge of the treatment snout. These block the protons outer transverse region of the lateral spread. Often two or three apertures are used in treatment, depending on the energy of the beam used (higher energy beams require a greater thickness of attenuator to block the field). The compensator is placed immediately after the apertures. This allows proton beams to be molded to three-dimensional objects, such as tumors. The compensator is usually made of acrylic and shaped to the distal edge of the field using a computer-controlled raster drilling pattern.

1.5.3.2 Spot Scanning

For scanning proton beams, a pencil beam is

For the PTC-H's spot scanning system, the

1.5.4 Dose Uncertainties

The range can be a source of uncertainty with proton beams. If the energy modulation is not accurately implemented or achieved, the SOBP may deviate from what is expected. This can result in underdosing the target or overdosing normal tissue.

There is also uncertainty introduced by the heterogeneity of the absorbing materials. The manner in which the proton beam range is varied mirrors the way in which the range can be changed in other absorbing materials, such as the human body. A section of high or low density tissue can cause a shift in the range of protons if not properly accounted for in treatment planning models. If the treatment planning system does not accurately model the heterogeneities of the absorbing tissues, the dose delivered could be different from what is predicted. This demonstrates the need for stringent quality assurance and attention to detail on the part of the radiation therapy team.

1.5.5 Beam Monitoring

As the beam modulators cause variability in

1.5.6 Dose Distribution Measurements

In addition to monitoring the beam output, it is important to characterize the dose distribution of the proton therapy systems to have an illustration of the behavior of the beam for treatment planning and delivery purposes. As mentioned in the previous section, ion chambers can be used to monitor the beam output at the treatment head as well as depth dose profiles. 2D dose distributions can be captured using either radiochromic film or 2D ion chamber arrays (24, 26). The measurements of 2D dose distribution are useful in patient specific QA at proton therapy facilities.

1.5.7 Proton Therapy in Treatment of Brain Tumors

When developing the phantom, some thought

Meningiomas arise from the meninges, or

Proton therapy in particular is a good treatment

2 Methodology

2.1 Phantom Design

2.1.1 Previous Phantom Designs

As part of the RPC's role in remote monitoring of institutions that participate in clinical trials, the center has created a number of mail-able dosimeter systems and phantoms. The phantom program at the RPC has utilized a variety of creative scientific minds to create heterogeneous phantoms for different regions of the body. There is an obvious advantage to heterogeneous over homogeneous phantoms, as the body itself has a diverse composition. More specifically, the RPC strives to create anthropomorphic heterogeneous phantoms, which are not only varied in their composition, but mimic anatomical composition. Some anthropomorphic phantoms, such as the one developed at the RPC for the evaluation of Intensity-Modulated Radiation Therapy (IMRT), are constructed with a tissue-equivalent surface and filled with water, while materials are placed inside with tissue-equivalence to tumors and/or critical structures (31, 32). Water is a good option for tissue-equivalent material, but it can be problematic. Air bubbles in the water in the phantom can cause discrepancies in imaging, treatment simulation, and dosimetry. In addition, water residue can cause mold to form in crevices of the phantom material if not properly cleaned. This is particularly the case in a phantom that includes real bones, such as a human skull.

The Alderson Average-Man phantom was created with a human skeleton cast in a synthetic isocyanate rubber (33). The material of the phantom is tissue-equivalent and durable, and can be cast around human bone as well as carved to represent anatomical airways, making it a good option for a phantom to be sent to a customer or external institution.

Phantoms designed by the RPC use various

2.1.2 The Anthropomorphic Head Phantom

Because there is still some uncertainty as to the

The phantom for this project was created with

Once the materials were measured and deemed

Axial CT images of the phantom were obtained

Figure 2.1. Head phantom

A hole of 7 cm in diameter was drilled

Figure 2.2. Insert hole in phantom

The imaging insert was developed for the

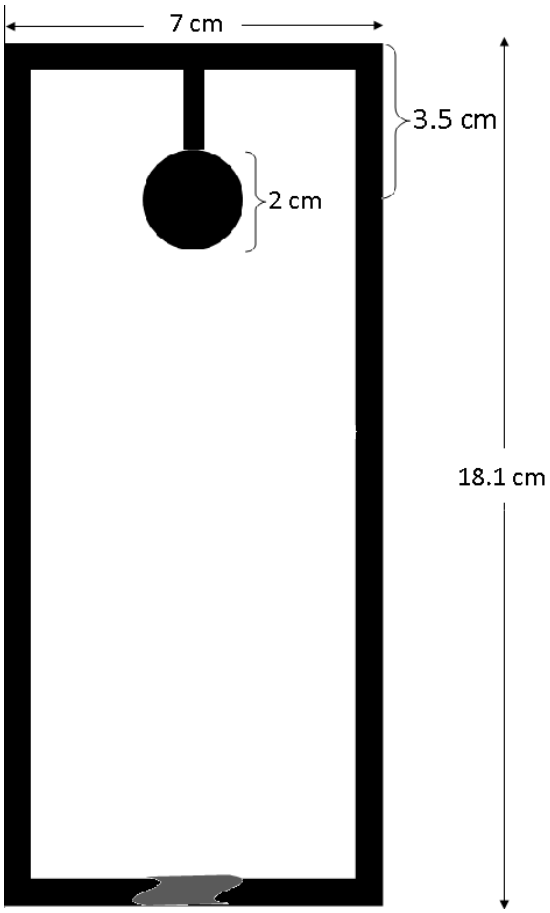

a. **b.**

Figure 2.3. MRI insert sketch (a.) and physical insert (b.), made of hollow acrylic with nylon ball suspended from the superior surface

The CT/irradiation insert is designed as a high

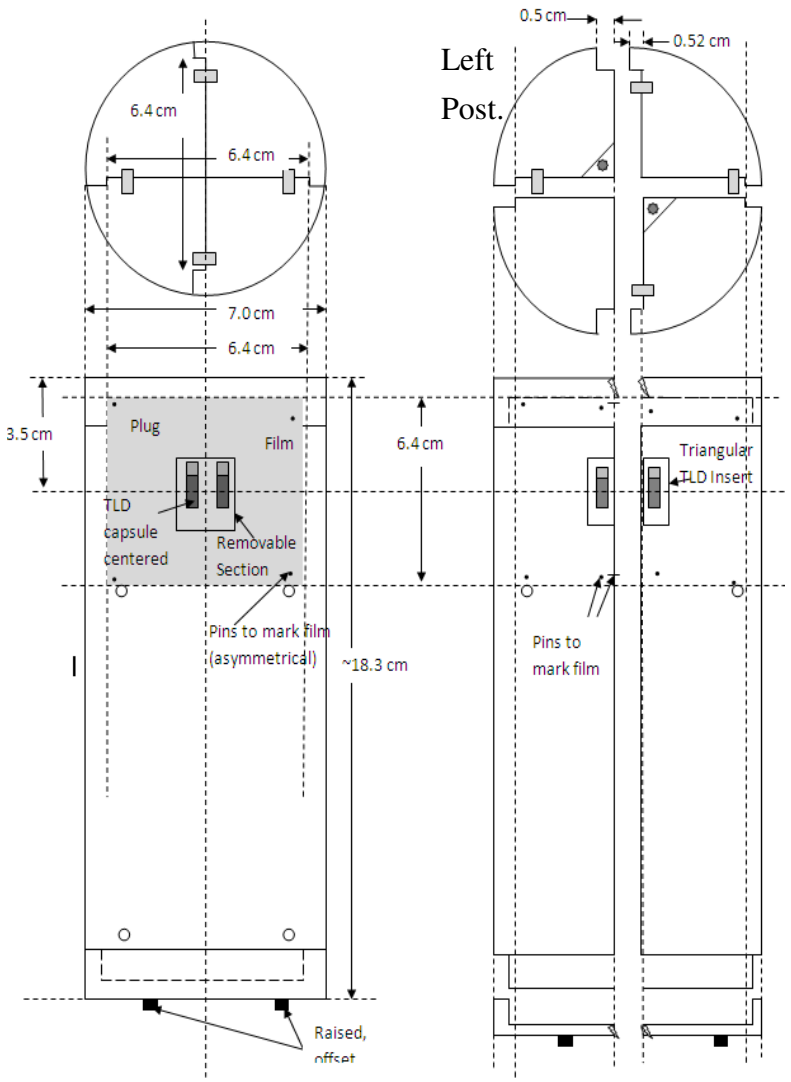

Figure 2.4. Dosimetry insert schematic of
This insert does not have a tumor embedded,

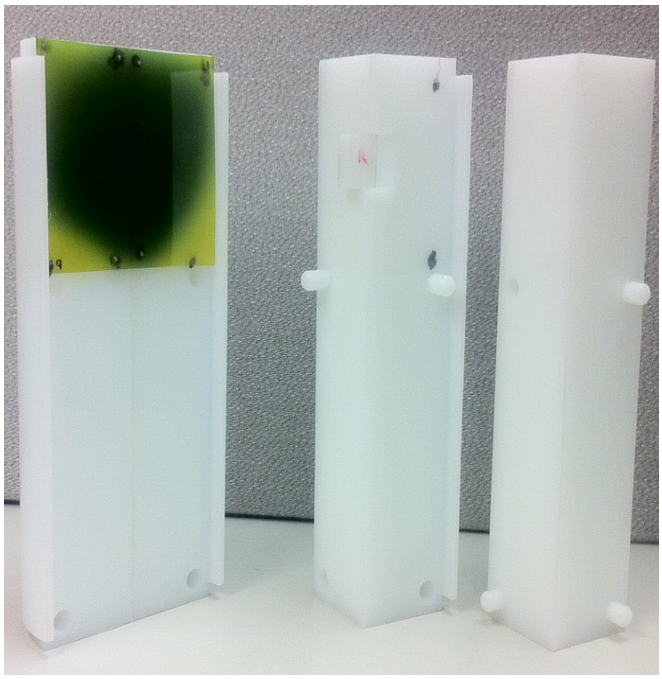

Figure 2.5. Solid polyethylene dosimetry insert, with irradiated film and right TLD capsule shown

Once the phantom is created, the next step is to

2.1.3 Determining Tissue Substitutes for Proton Therapy

To design the heterogeneous phantom, it was

The relative stopping powers of potential phantom materials were determined with the passive scattering proton beams at the UT MD Anderson Proton Therapy Center of Houston (PTC-H). The materials studied consisted of two different types of epolene, Mix D plastic, a solid wax, and the solid material that makes up Alderson Rando phantom material, all of which are supposedly water-equivalent materials (with respect to photon therapy).

The PTC-H's 3D PTW MP3 scanning water

At each measurement position, a four second

In order to determine the relative stopping

Once the data were recorded for both the water

To calculate the relative stopping power of each material, the depths of the distal 80% points were calculated using a linear slope formula between the two data points straddling the distal 80% for both the water only and water plus slab depth dose curves. It

is the preference of some to use the distal 90% points instead (35). However, it was recommended that for the purposes of this experiment the distal 80% be used (36). As long as the same two percent depth dose points are being compared, the relative stopping power relationship will hold because only the shift in depth between the two depth dose curves is being observed, and all points along the curve should shift by the same amount. A linear regression was performed on the distal 80% points. Then, the relative stopping

$$\frac{PDD\ shift}{material\ thickness} + 1$$ Equation 2.1 (37).

$$RLSP = \left(\frac{PDD\ shift}{material\ thickness}\right) + 1 \qquad \textbf{Equation 2.1}$$

A relative stopping power close to unity was desirable (meaning the material had a stopping power close to that of water).

The phantom materials of interest were scanned with the Proton Center's CT machine, a GE LightSpeed RT16 (GE Healthcare, Waukesha, WI) to measure their Hounsfield units. The materials were taped to the CT machine table which was aligned with the lasers. An imaging technique of 120 kV and 300 mAs was used for the CT scans of epolene and Mix D, while 120 kV and 350 mAs were used for "wax" and Alderson material. The difference in technique was due to different technologists operating the machines, but the small variation in mAs should not affect the CT number of the materials, so the discrepancy was not a concern for the measurements. For both imaging techniques, the scans were done in the fast helical setting with a pitch close to 1 and using the head Scan Field of View. The CT numbers were obtained using the Eclipse treatment planning system (Varian Medical Systems, Palo Alto, CA), taking the average of 10 measurements made across a central image of the material.

Once the RTOG 0539 protocol was reviewed, it was determined that to stay true to common meningioma treatment procedures, the phantom needed to be imaged with MRI for treatment planning. It was unclear initially whether or not the phantom material would show up on an MR image due to its solid state. To determine whether or not this was the case, an old anthropomorphic phantom from the RPC was imaged to see if any parts were visible or distinguishable. A GE Signa HDxt 1.5 Tesla research scanner (GE Healthcare, Waukesha, WI) at MD Anderson Cancer Center was used. The phantom was placed in the supine position in an 8 channel array head coil. An initial localizer scout was performed to see if any signal was detected. A fast spin echo was used due to the

short time of T_2* of solid materials. When a signal was detected, a second image was obtained for an axial cross section of the mid-skull area. Surprisingly, a fairly detailed image was obtained from this scan in which the outer shape of the phantom as well as bony anatomy and air pockets inside were easily visible. An image with a greater scan extent was then obtained using a more pertinent scan setting with a steady state free precession acquisition, which for the GE machine was 3D Fiesta C. The contours of bone, phantom material, and air were all still visible.

For MR images for treatment planning, RTOG 0359 recommends obtaining T1, T2, FLAIR, and postcontrast multiplanar T1 images (12). The protocol says Gadolinium contrast agent should be administered per institutional policy. Both of these recommendations should be kept in mind for patient imaging, but were impractical for phantom imaging, and as will be discussed further in Section 2.3.1.1, only one MR sequence image set was used for the phantom simulation and treatment planning.

2.2 Developing the Phantom Components for Precise Setup

Patient setup was an important part of developing the phantom. For reproducibility purposes, it was desired that the phantom have some kind of apparatus that would allow for the precise setup of the phantom for imaging and treatment. Other phantoms at the RPC have features such as an extended base at the neck or leveling screws that support the head and neck phantom in a way such that it is positioned similar to a real patient's head and neck during treatment.

Per the recommendation of the PTC-H, the head & neck phantom was placed in the supine position. The PTC-H treatment protocol also recommends using a Head & Neck mask, head rest, and bite block, but it was determined that for ease of setup and accessibility to the dosimetry insert during re-loading, these accessories would not be employed. Instead, leveling screws were designed and incorporated into the base of the phantom in the posterior, inferior region.

2.3 Testing the Phantom

2.3.1 Phantom Simulation

2.3.1.1 MRI Simulation

As with the phantom material scan, the MRI simulation for target delineation was performed on a GE Signa HDxt 1.5 Tesla scanner. The MR phantom insert, containing the nylon "tumor," was carefully filled with tap water so as to minimize the number of air bubbles. Once the insert was placed in the phantom, the phantom was placed in an eight channel array head coil. The head was placed in the supine position, with the posterior leveling screws extended for balance. Foam blocks were placed on each side of the head to reduce vibration while the scan was being performed. The phantom was aligned such that the localizing lights were aligned to the center of the head, using the medial commissures of the eyes along the axial direction, and the center of the nose in the sagittal direction.

A 3-plane localization was performed first to ensure proper setup. Several series were acquired, but the 3D SPGR, GE's version of an RF spoiled gradient echo, was used for treatment planning purposes. This series matched the volumetric CT best for fusion, and contained a well-delineated image of the target. An axial slice of the MR image set demonstrates the target delineation in Figure 2.6:

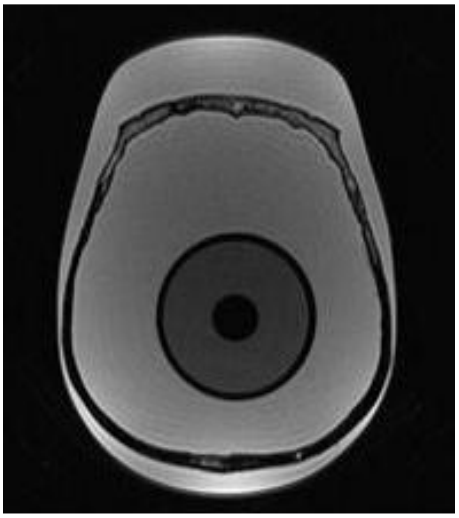

Figure 2.6. 3D SPGR MR image at the center slice of the target

2.3.1.2 CT Simulation

The CT images were acquired using the proton-dedicated GE LightSpeed RT16 scanner at the PTC-H. The dosimetry insert was loaded with TLD and film and placed inside the phantom. The phantom was placed directly on the CT table in the supine position. The posterior leveling screws were adjusted so that the head was supported in a patient-like simulation fashion. Three pieces of tape were place on the head: one near each of the left and right temples, and one in the center of the forehead. The laser lines were marked on the tape, and small plastic bbs were placed at the vertex of each tape line. A typical proton center head protocol was used for the CT simulation. An axial slice of the target region of the CT images is shown in Figure 2.7, where the TLD capsules are delineated.

Figure 2.7. CT image at the center slice of the target region

The images were transferred to the PTC-H's Eclipse treatment planning system. In Eclipse, the CT table was digitally replaced with the proton treatment couch. This was done using an in-house DICOM digital couch replacement algorithm that runs through a MATLAB application.

2.3.1.3 Image Fusion

The MR scan identifying the target and structures had to be fused with the CT image to identify the target within the CT images to complete the treatment planning and dose calculation process. For the image fusion, the Eclipse mutually shared algorithm

was used. The region of interest was limited to the head. The algorithm's registration uses "manual tools" to translate the images for a generic match, then pixel registration for a more detailed fusion guided by bony anatomy alignment. The "blend with" view can be used to slide over the MR and CT images to see how closely the algorithm matched the images.

2.3.2 Treatment Planning

Once an acceptable fusion was achieved, the target volume was contoured. The 2 cm diameter ball was designated as the GTV, and the PTV was created with a 0.5 cm expansion in all directions, per RTOG 0539 specifications. Both passive scattering and spot scanning proton beam plans were created. The dose prescription was 54 CGE, but for the purposes of the project, the plans were created to deliver 5.4 CGE to the target volume one time. This is a dose one-tenth the size of the prescribed dose was given to the phantom target, per typical RPC protocol for head & neck phantoms (31). This lower dose was chosen to accommodate the dose range of the Gafchromic film used in the dosimetry insert. Per the RTOG 0539 specifications, all dose constraints were scaled to 10 percent of their original values. This meant that the 5.4 CGE must cover $\geq 95\%$ of the PTV, that the minimum dose to the PTV be at least 5.1 CGE, and that the maximum dose to any point (≥ 0.03 cc) not exceed 6.2 CGE (12). Treatment plans were created using both the passive scattering and spot scanning proton beams at the PTC-H. Digitally Reconstructed Radiograph (DRR) images were also created in the treatment plans for comparison with radiographs that were to be acquired before each treatment for localization purposes.

2.3.2.1 Passive Scattering Plan

The passive scattering plan was designed using three beams: a posterior-anterior, left vertex, and right vertex beam. The beams were equally weighted to deliver 5.4 Gy (5.94 CGE) and combined to form a rough-edged uniform-dose sphere surrounding the target volume. It is important to note that the passive scattering treatment plan was initially designed with the intention of delivering 5.4 CGE to the target. However, when the MU calculations were performed, the RBE was not accounted for and the dose delivered to the phantom target was actually a physical 5.4 Gy.

The isodose distributions are shown in Figure 2.8, and the beam parameters are listed below in Table 2.1.

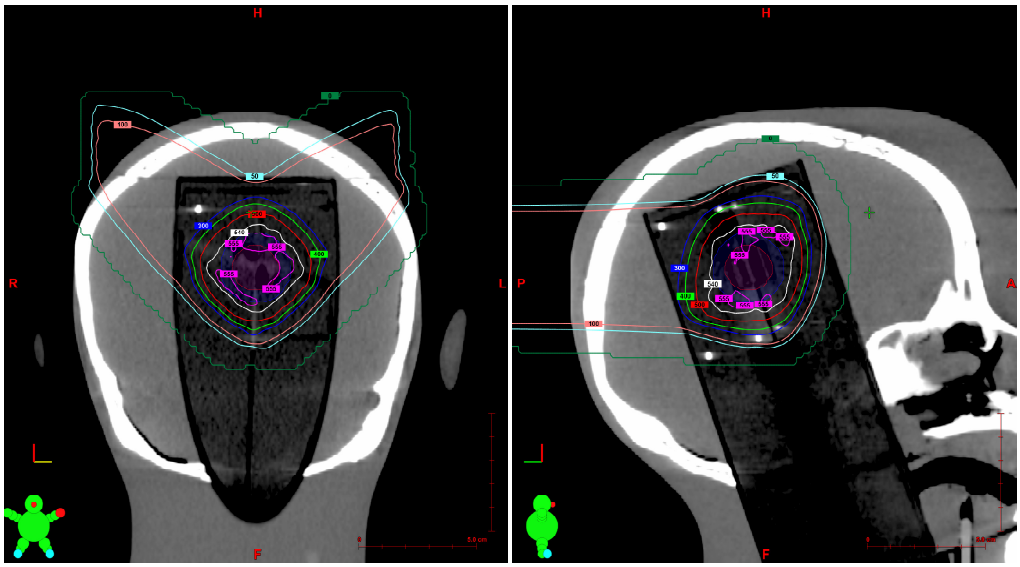

a. **b.**

Figure 2.8. Passive Scattering treatment plan shown in the coronal (a) and sagittal (b) planes

Passive Scattering Treatment Plan			
Prescribed Dose: 540 cGy			
Beam	A	B	C
Beam Name	Posterior-Anterior	Left Vertex	Right Vertex
Beam Energy [MeV]	160	140	140
Gantry Angle	180º	75º	285º
Couch Angle	0º	320º	40º
Snout Position [cm]	30	25	25
Dose to isocenter [cGy]	181.9	181.3	182.2

Table 2.1. Passive Scattering treatment plan parameters

For each field, two brass apertures (Figure 2.9) and one compensator (Figure 2.10) were created at the in-house PTC-H machine shop and checked against the treatment plan specifications.

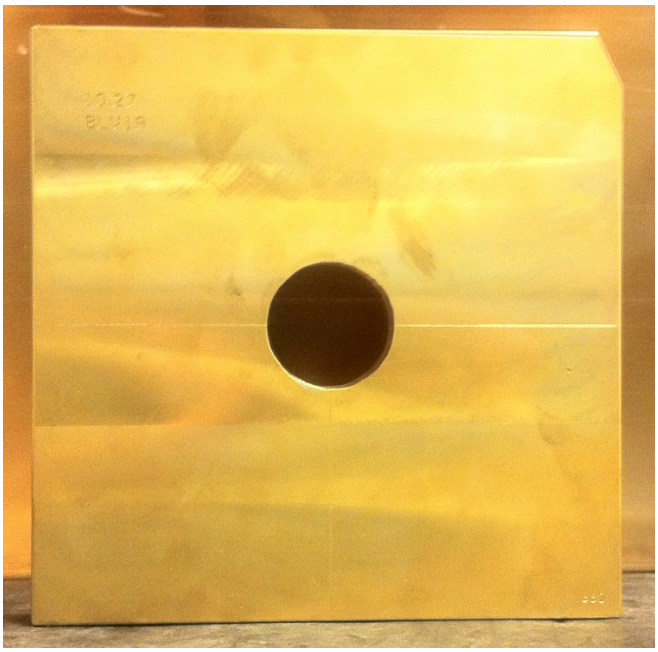

Figure 2.9. Passive Scattering beam aperture

Figure 2.10. Passive Scattering beam compensators for (from left to right) beams A, C, and B

The phantom was irradiated on the G1 passive scatter gantry at the PTC-H. The treatment plan for the phantom had been created for the G2 gantry, so despite the beams being matched (within one percent), the Digital Imaging and Communications in Medicine (DICOM) commands had to be converted to the right syntax for the G1 gantry. This was accomplished by using a DICOM editor and changing the beam modulation ID from 84 to 20 for the 160 MeV beam, and from 85 to 21 for the 140 MeV beam, as well as a few other beam identifiers.

The monitor units (MU) were calculated for each field based on

$$MU = \frac{Dose}{Energy\ OF * Range\ Shifter\ Factor * SOBP\ OF}$$ Equation 2.2:

$$MU = \frac{Dose}{Energy\ OF * Range\ Shifter\ Factor * SOBP\ OF} \quad \textbf{Equation 2.2}$$

The relative output factor, range

Passive Scatter Treatment Plan			
Prescribed Dose: 540 cGy			
Beam	A	B	C
Dose to isocenter [cGy]	181.9	181.3	182.2
Relative Output Factor	0.865	0.927	0.927
Range Shifter Factor	0.967	0.981	0.996
SOBP Factor	1.295	1.073	1.073
MU Delivered	**167.4**	**185.3**	**182.0**

Table 2.2. Monitor Unit (MU) parameters for the passive scattering treatment fields

2.3.2.2 Spot Scanning Plan

The spot scanning plan was designed using the

a. **b.**

Figure 2.11. Spot scanning treatment plan shown in the coronal (a) and sagittal (b) planes

The beam parameters are listed below in

Spot Scanning Treatment Plan		
Prescribed Dose: 540 CcGyE		
Beam	A	B

Beam Name	Left	Right
Nominal Beam	108	113.4
Nominal SOBP	3.2	3.37
Gantry Angle	90º	270º
Couch Angle	315º	45º
Snout Position	38	38
Dose [CcGyE]	270	270
MU	63.6	62.5

Table 2.3:

Spot Scanning Treatment Plan		
Prescribed Dose: 540 CcGyE		
Beam	A	B
Beam Name	Left Vertex	Right Vertex
Nominal Beam Energy [MeV]	108	113.4
Nominal SOBP Width [cm]	3.2	3.37
Gantry Angle	90º	270º
Couch Angle	315º	45º
Snout Position [cm]	38	38
Dose [CcGyE]	270	270
MU	63.6	62.5

Table 2.3. Spot scanning treatment plan parameters

The phantom was irradiated on the G3 spot scanning beam at the PTC-H on. The monitor units for this plan are calculated by the Eclipse treatment planning system, so a manual MU calculation was not required for this plan, as was the case for the passive scattering plan.

2.3.3 Treatment Delivery

2.3.3.1 Passive Scattering Irradiations

The phantom was set up in the supine

Orientation	Nozzle	Cage
kVp	65	65
mA	630	500
ms	80	60

Table 2.4. kV imaging parameters for PTC-H proton treatment setup

The x-ray images were compared to DRRs

The first passive scattering irradiation trial

Once the first trial irradiation was delivered,

Once the phantom was reloaded with unirradiated dosimeters, it was repositioned on the treatment couch using the lasers to align with the new tape markings. For the second irradiation trial, the leveling screws at the base of the phantom were adjusted so the tape markings aligned with the lasers, as it was determined that the screws had been bumped during reloading. Another set of x-rays was acquired to verify the positioning of the phantom. No adjustments were made to the phantom or the couch. The film and TLD were reloaded again for the third trial irradiation, and the fields were verified with x-ray images.

2.3.3.2 Spot Scanning Irradiations

For irradiation, the dosimetry insert was

The treatment plan had been designed to deliver 54 CGE over the course of 10 fractions, so only the first fraction was delivered for each trial, for a dose of 5.4 CGE. The first spot scanning irradiation trial was irradiated according to the treatment plan, with the left vertex beam, beam A, delivered first. Beam A had a gantry angle of 90º, a couch angle of 315º and a nominal beam energy of 108 MeV. Beam B, the right vertex, was delivered next, with a gantry angle of 270º, a couch angle of 45º, and nominal beam energy of 113.4 MeV, which is the energy of the proton spots with the distal 90% range at the deepest layer.

Once Trial 1 irradiation was delivered, the phantom was removed from the couch and reloaded with TLD and film. Again, x-ray imaging was used to assess phantom alignment before the doses were delivered and calculate necessary couch shifts. The same procedure was followed for the third trial as well.

2.3.4 TLD

2.3.4.1 Absolute Dose Determination

The RPC has developed a mailable TLD

Thermoluminescent dosimeters were used to measure

$Tm \times S \times E \times L \times F$ Equation 2.3 will be used:

$$Dose = \frac{T}{m} \times S \times E \times L \times F \qquad \textbf{Equation 2.3}$$

The dose measured from TLD is calculated

The sensitivity correction factor is perhaps the most important as it can vary between individual readout sessions due to factors such as system electronics and the reader planchette (41). The correction factor looks at the system sensitivity (dose per reading) of a specific batch of TLD. *S* is usually calculated by irradiating TLD to a known dose (using an ion chamber measurement for reference) and reading out these TLD both before and after the TLD reading session. This factor can be measured by dividing the known dose by the TLD response for those measurements (*T'*) and $\boldsymbol{Dose_{known}T' \times L' \times F'}$ Equation 2.4:

$$\boldsymbol{S = \frac{Dose_{known}}{T' \times L' \times F'}} \qquad \textbf{Equation 2.4}$$

where *L'* and *T'* are the relative linearity and fading factors of the TLD powder batch.

The energy correction factor takes into account that TLD crystals have a small energy dependence. The factor is found by comparing the output per dose of a TLD at a ^{60}Co energy (reference energy) to the energy of a proton beam. This TLD proton energy correction factor was determined to be the same for all proton energies tested by the RPC and is unity.

The linearity correction factor accounts for the slight non-linearity of TLD response over a wide range of doses. To find this correction factor, several TLD were irradiated over a range of doses. For low doses, there is a linear adjustment that needs to be made, but at higher doses, the relationship becomes logarithmic. In the dose range we used, the linearity correction factor is found with inverse of response of the TLD response v. dose curve, as described in the following $\boldsymbol{L=a*Dose+b}$

Equation 2.5:

$$\boldsymbol{L = a * Dose + b} \qquad \textbf{Equation 2.5}$$

where *a* and *b* are coefficients specific to each batch of TLD.

The fading correction factor takes into account the recombination of some electron-hole pairs before the TLD dosimeter is read out. The RPC uses a double exponential fading correction factor based on a plot of time v. percent of signal obtained in readout:

$$\boldsymbol{F = \frac{1.31314}{ce^{-dt} + fe^{-gt}}} \qquad \textbf{Equation 2.6}$$

The change in the fading correction is minimized by waiting a minimum of 14 days after irradiation to read out the dosimeters. The RPC uses the same fading curve for all batches of TLD as there is little variation in this correction factor when the minimum readout time is standardized.

The TLD in the phantom for each irradiation consisted of two double-loaded LiF TLD-100 dosimeters (Quantaflux, LLC, Dayton, OH). Each capsule was placed 3 mm off axis, one above and one below the center line.

2.3.4.2 TLD Characterization

The TLD batch used for the project was named batch B07 and had been characterized by the RPC prior to irradiation. As discussed in the previous section, correction factors are needed for calculation of TLD dose. For the linearity correction factor for the batch of TLD used the slope (*m*) and y-intercept (b) found in $\boldsymbol{L=a*\ Dose+b}$ **Equation 2.5** are -0.00027842 and 1.08353, respectively. For the fading correction factor, the $\boldsymbol{F=\frac{1.31314}{ce^{-dt}+fe^{-gt}}}$ Equation 2.6 parameters are listed in Table 2.5.

N	1.3493
a	1.2815
b	0.00010885
c	0.06781
d	0.071908
x	Days between irradiation and reading

Table 2.5. TLD fading correction factor constants

2.3.4.3 TLD Evaluation

The TLDs were read out after 21-23 days, so as to minimize the effects of fading. The TLD was read in between a series of standard and control TLD which had been irradiated using the ADCL's ^{60}Co machine. An unexposed TLD-100 pack was used as the background, and its reading was subtracted out from the readings of the exposed TLD. $\boldsymbol{Dose=\frac{T}{m}\times S\times E\times L\times F}$ Equation 2.3 was then used to calculate the dose delivered to each TLD. TLD have been found in some cases to underestimate proton

dose by about 7%, but this is mostly due to positioning errors (38). In a previous study done by the RPC for the development of a head & neck phantom, TLD dosimeters were found to have an accuracy of ± 4% and precision of ± 3% at a 90 % confidence interval (31).

For this experiment, a ratio between calculated TLD dose (based on the treatment planning model) and measured TLD dose would be deemed acceptable within the range of 0.95-1.05 in order to meet the 5% point dose agreement criterion. The coefficient of variation was used to calculate reproducibility, and COV values of less than 3% were considered passable.

In order to test statistical significance of the TLD results, a one-sample t-test was performed with a significance level of 0.05. The t-test values was computed using the equation below (42):

$$t = \frac{\bar{x} - \mu_o}{s/\sqrt{n}} \qquad \textbf{Equation 2.7}$$

where $\bar{x}$ is the mean ratio of calculated v. measured TLD dose, μ_o is the null hypothesis, which we define to be 0.949 (outside of the 5% limit), where s is the standard deviation and n is the sample size, three trials. The critical value was found using the TDIST function, which yields the probability for a t-test distribution. The statistical significance was found by finding the p-value, which if less than 0.05 was said to be statistically significant. If the p-value was greater than 0.05, the data would be considered not statistically significant, and the hypothesis would be rejected.

2.3.5 Film

Another passive dosimeter that can be used effectively in a mailable monitoring program is radiochromic film. The RPC already uses this film as part of its mailable dosimetry program. Radiochromic film is a good option for finding the dose distribution of a radiation beam, as it exhibits no angular dependence, a high spatial resolution, and a low spectral sensitivity (31). Another advantage of radiochromic film is that it is tissue-equivalent, so as a beam passes through it, the behavior of the particles shouldn't be disrupted (43).

Gafchromic® EBT2 is yellow in color and uses a

Polyester Overlaminate (50 µm)
Adhesive (25 µm)
Topcoat (5 µm)
Active Layer (20 µm)
Polyester Substrate (175 µm)

Figure 2.12 Design of Gafchromic® EBT2 film showing the various layers of the film

One advantage of EBT2 film over

In order to assure accuracy of the film measurements, the film was calibrated with a passive scatter beam at the PTC-H. Six doses were chosen for irradiation: 50, 150, 250, 350, 550, and 750 CcGE. These doses were chosen because they are the standard doses delivered for photon beam calibrations at the RPC. The MU necessary to reach each dose

$Dose RBE * Energy\ OF * Range\ Shifter\ Factor * SOBP\ OF$ Equation 2.8:

$$MU = \frac{Dose}{RBE * Energy\ OF * Range\ Shifter\ Factor * SOBP\ OF} \quad \textbf{Equation 2.8}$$

The measurements were taken in a water tank. A range shifter was not used for these measurements, so the range shifter factor in this case was 1. An SOBP of 5 cm was used, and the film was placed in the middle of the SOBP, perpendicular to the beam. An ion chamber was placed in the field for reference. The six dose measurements were collected for beam energies of both 140 MeV and 160 MeV, the energies of the passive scatter treatment beams.

The films were scanned using the red light CCD Microdensitometer for Radiochromic Film Model CCD100 (Photoelectron Corporation, Lexington, MA) at the RPC. A flat field adjustment was made using a blank piece of film from the same batch. The average optical densities were obtained for each dose using ImageJ software (Rasband 1997-2011), and a calibration curve was created with a third degree polynomial fit.

It was determined that creating a proper dose response curve for the spot scanning system was beyond the scope of this project. Other studies, such as one performed by Zhao *et al.*, have found the OD-dose calibration curve of spot scanning systems similar to that of scattered beams (46). As such, it was decided that a measurement of a uniform field of a known dose with the spot scanning system could be compared to the passive scattering dose response curves, and if that dose was within 5% of what was predicted by

the polynomial fit, the passive scattering dose response curve would be used. A uniform 10x10 cm^2 spot scanning beam with an SOBP of 10 cm was delivered to a piece of film from the same batch. The OD-dependent dose measured was compared to the dose delivered.

Film was placed in the coronal and sagittal planes of the dosimetry insert in order to observe the dose distribution of the proton treatment. The film was all cut using the same template, and each coronal piece was cut in half to allow the sagittal piece to intersect it in the middle of the target location.

EBT2 film should always be scanned in the same direction and with the same orientation. To ensure this process, the pieces of film were marked with permanent marker in the outer corners, indicating orientation. It was recommended by International Specialty Products, the manufacturer of this film, that the film rest for at least 24 hours before being read out to ensure dose accuracy (44). The films used in the phantom irradiations were read out after two days.

2.3.6 Film, TLD, & CT Registration

The film and TLD needed to be registered with the CT images for analysis between the treatment plan dose clouds and dose delivered. The RPC uses in-house developed software called rpcfilm that registers CT images and the dose distribution with TLD and film locations and the corresponding measured dose distributions.

Pin pricks on the film provide spatial orientation and convenient registration points for the program. It is necessary to set a central axis and measure the distance between the pin pricks and that origin. This was done using the isocenter of the target as the origin. Pricked pieces of film were placed on grid paper for alignment and the coordinates of the pin pricks were measured using calipers. These coordinates were entered into the excel file under the corresponding “sagittal” and “coronal” labels. The CT images were registered to the system by setting the center of the target as isocenter and measuring the distance to four pins in the dosimetry insert.

Once the irradiated film has been scanned into the system and is pulled up in rpcfilm program, the pin-pricks can be identified and the spatial orientation of the film is registered on one coordinate system, as delineated in Figure 2.13. The CT image set is

opened with Computational Environment for Radiotherapy Research (CERR) software and pins are used to mark the spatial coordinates and register the images to a second coordinate system. The program then uses the program CERR to register both the film and the CT image set to a third set of coordinates so that the two can be compared.

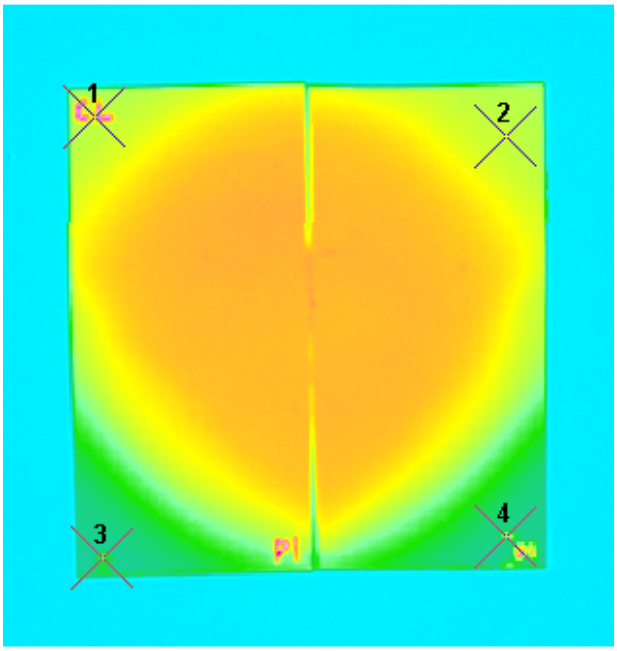

Figure 2.13. Pin pricks from coronal film picked for registration with pre-measured points

When the registration occurs for both the film and the treatment plan image coordinate systems, error in the form of root mean square (RMS) is calculated by the rpcfilm program to assess the goodness of fit. The upper limit on the RMS for our point registration was set at 1mm so as to minimize propagation of error. These errors are recorded as "RMS Error" for film registration and "RMS 3D" for CT image registration, as shown in Figure 2.14.

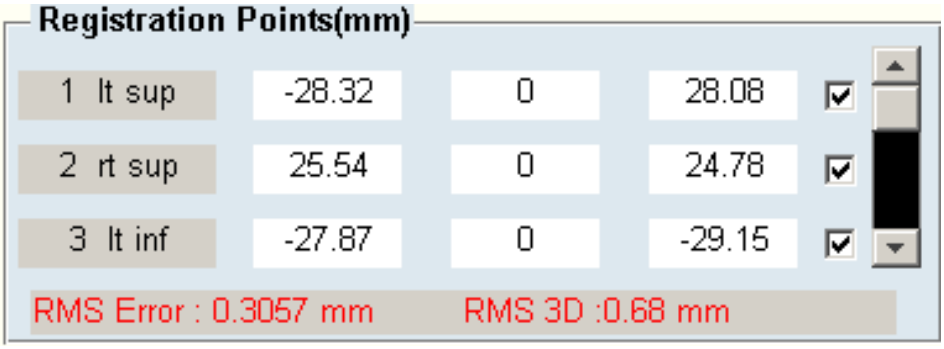

Figure 2.14. The RMS errors for film and CT registration, as displayed in MATLAB

When the film is properly registered, a dose response calibration curve is applied to convert the optical density of the film to dose. The TLD positions are also recorded based on the center of the active portion of the capsules in relation to the film coordinate system. The dose grid of the film is scaled using the TLD dose, which is applied to the points on the film where the TLD capsules have been assigned. The doses for the rest of the film profile adjust accordingly.

2.3.7 2D Gamma Analysis

The agreement between 2D dose distributions was evaluated using a gamma analysis procedure, with dose or distance agreement criteria of both ±5%/3mm and ±5%/5mm. The comparison analysis can be performed once the CT data and film had been registered. A data omission mask was applied to regions of the film that we did not want included, such as the pin pricks, pen marks, and the strip between the two pieces of coronal film, as seen below in Figure 2.15. The RPC uses a pixel pass rate of 85% for gamma analysis, so the same criterion was used for this project.

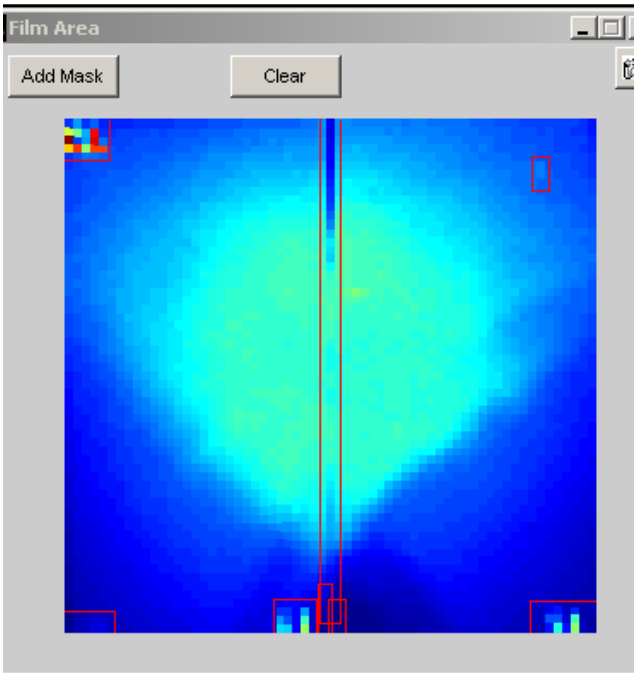

Figure 2.15. Masks applied to the coronal film to avoid comparison between compromised areas

2.3.8 Distance to Agreement Measurements

With the dose profiles created by the gamma analysis in the rpcfilm program, distance to agreement (DTA) measurements could be calculated between the treatment planning system and the delivered dose profiles. These measurements were calculated in the regions of steep dose fall-off beyond the target. This is done by fitting a regression line to the dose fall-off regions, starting at the 80% dose point and extending to down as far as the 30% dose point. The distance in millimeters is then measured between where these dose points fall in the planned dose distribution and on the film. An average displacement for each side of the target is then calculated (i.e. +/- mm shift left/right, superior/inferior, anterior/posterior). With our gamma analysis acceptance criteria of ±5%/3mm, it is desired that the DTA measurements are less than 3 mm, and less than 5 mm for the loser ±5%/5mm criteria. While the gamma analysis tells us the percentage of pixels that pass the criteria, the DTA measurement quantifies the average shift between treatment planning dose and delivered dose.

3 Results

3.1 Phantom Materials

3.1.1 MR Insert Materials

For the MR phantom insert, the relative stopping power and CT numbers were irrelevant to the selection of the materials, as this insert will not be irradiated with the proton beam, nor imaged with CT. Acrylic was chosen for the shell of the MR insert and the cylinder was left hollow to be filled with water. The target was made of a nylon sphere with a diameter of 2 cm, as discussed and shown in Section 2.1.2.

3.1.2 Material Stopping Powers and HU

Recalling that the purpose of the first specific aim was to find materials with relative stopping powers (RSP) and CT numbers close to those available in the treatment planning system calibration curve for tissue substitute materials, several tested materials will be discussed in this section. The complete results of the relative stopping power and HU measurements are shown below in Table 3.1.

Materials	Relative Stopping Power	CT Number [HU]
Alderson Material	1.00	16 ± 5
Epolene	0.95	-122 ± 2
Mix D	-	-11 ± 40
Wax	1.04	7 ± 4

Table 3.1. RSP and CT Number of materials tested for the phantom

Epolene was found to have a promising relative stopping power as compared to water. However, the Hounsfield units for epolene were not close enough to water to allow for its use as a tissue equivalent material (-122 ± 2 HU). Another material, Mix D, had highly variable HU (range: -52 – 123 HU) due to the heterogeneity of the mix itself. As the material was not available in a more homogeneous form, it was determined ineligible as a tissue-equivalent material and thus not scanned with the proton beam. A waxy material was tested, and while its average HU was close to that of water (7 ± 4), the relative stopping power was not the closest to water of all the materials tested. The Alderson material was tested and found to have a relative stopping power and HU close to water, with a relative stopping power of 1.00 and a mean HU of 16 ±5. The proton depth dose curves measured in water with and without the Alderson material in the

beam's path that were used to determine the relative stopping power of the Alderson material are seen in Figure 3.1:

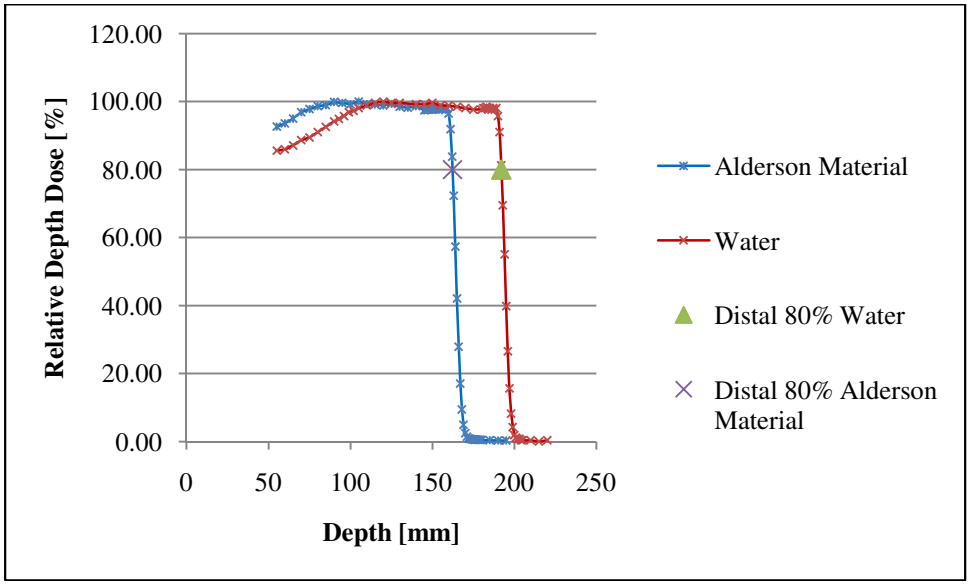

Figure 3.1. Depth dose curves of water and water with Alderson material present

Due to the water-like properties of the Alderson material, it was deemed acceptable as a water and soft tissue substitute for the phantom. Based on stopping power measurements taken previously by the RPC, high density polyethylene was chosen for the dosimetry insert. For the purpose of comparison to the treatment planning system, the RSP and HU of each material is graphed along with the PTC-H Eclipse treatment planning system calibration curve in Figure 3.2 (5, 35).

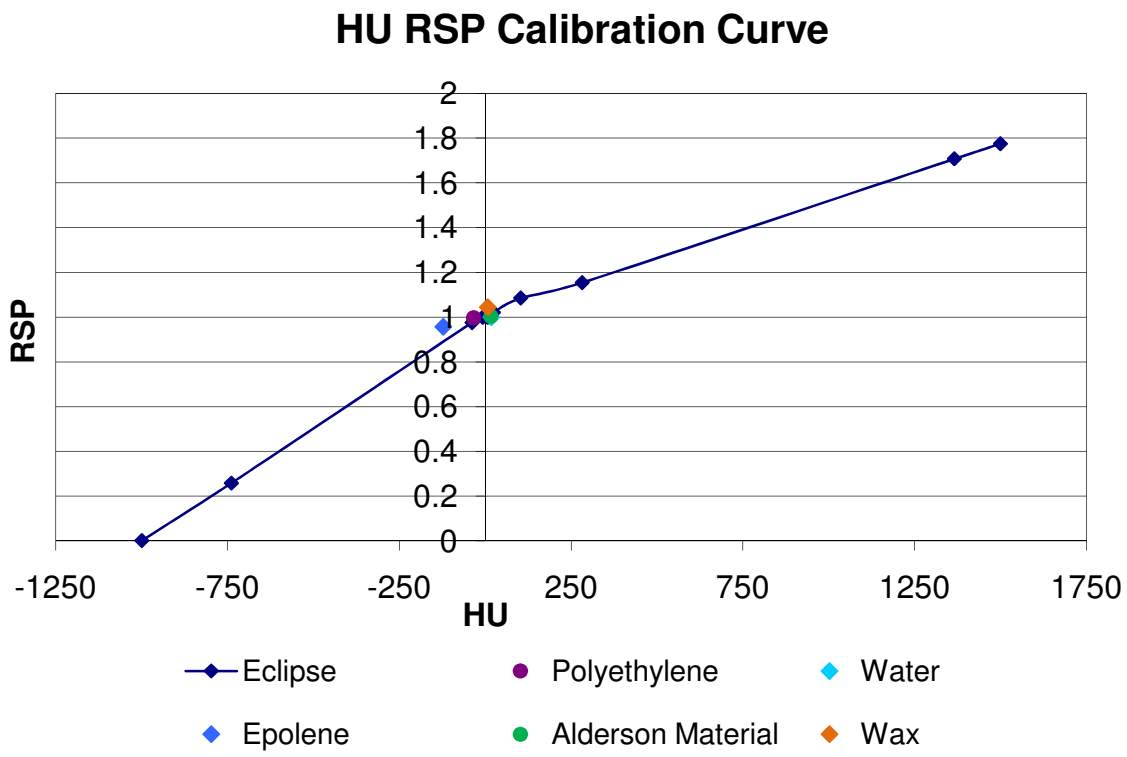

Figure 3.2. HU v. RSP of materials tested compared to PTC-H Eclipse treatment planning system calibration curve

The absolute error of the material thicknesses was 0.002 mm for each measurement, so the total error of the material thickness calculations was 0.004 mm. The depth dose scanning system is believed to be accurate within 0.1 mm. This gives a total error for the Relative Stopping Power of about 0.5%.

3.2 Film Calibration

The film calibration irradiations yielded dose response curves using passive scattering beams. The two dose response curves for 140 MeV and 160 MeV proton beams were compared and found to be essentially identical, as shown in Figure 3.3. Because of the similarity between the two curves, the 140 MeV curve fit was used for all data analysis. This curve was chosen because two of the three passive scattering beams used to irradiate the phantom were 140 MeV. The 160 MeV curve was only 1.5% different from the 140 MeV fit, while the "average" polynomial fit provided a 2.1% difference from the 140 MeV fit, so it was determined that the 140 MeV fit would be acceptable for all data, as it most closely represented the weighting of energies. The

greatest standard deviation of the optical density measurements was 0.014, and the COV centered around 1.0%. The equation used for film calibration in the CERR file is shown in Figure 3.3:

$$Dose = 29.429(OD)^3 - 4.1316(OD)^2 + 5.448(OD) \quad \textbf{Equation 3.1}$$

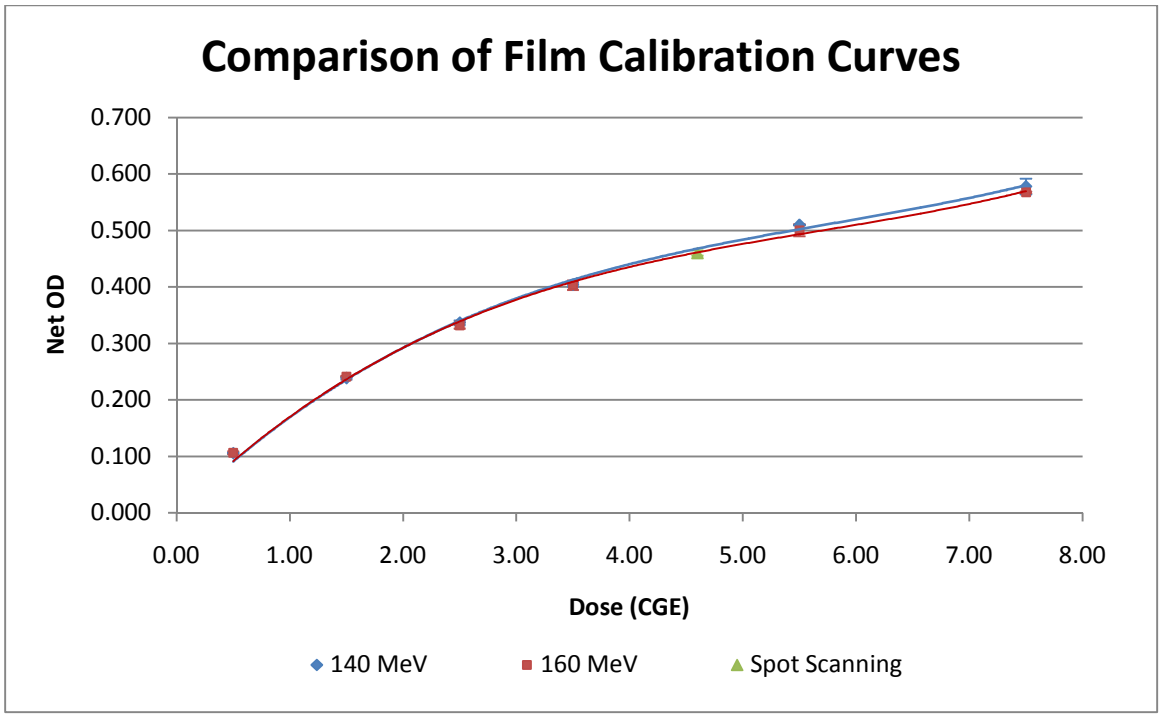

Figure 3.3. Gafchromic® film proton dose response calibration curves for 140 & 160 MeV passive scattering beams

For assessment of the appropriateness of the passive scattering dose-response curve for the spot scanning system, the optical density of a uniform field of irradiated film was measured. The calculated dose based on the passive scattering calibration curve was within 5% of the measured delivered dose, which was determined to be close enough to allow for the use of the 140 MeV polynomial fit for the spot scanning films as well. The actual dose determined by the film using the calibration curve is scaled by the TLD point doses. Thus, as long as our calibration curve can provide a dose from film that is close to the expected value, the absolute dose can be determined in conjunction with the TLD measurements.

3.3 Passive Scattering Phantom Dose Measurements

3.3.1 Absolute Dose Comparison

The phantom doses from each passive scattering irradiation trial were measured with TLD and compared to the calculated doses from the Eclipse treatment planning system. The right anterior TLD was expected to receive a physical dose of 540 cGy and the left posterior TLD was expected to receive 545 cGy. The values for the calculated and measured doses, as well as the ratio of the measured to calculated doses, are given in Table 3.2:

	Passive Scatter			
	TLD Location	Calculated Dose [cGy] - TPS	Measured Dose [cGy] - TLD	Meas./Calc. Dose
Trial 1	Right Anterior	540	520.9	0.965
	Left Posterior	545	527.8	0.968
Trial 2	Right Anterior	540	527.8	0.977
	Left Posterior	545	535.2	0.982
Trial 3	Right Anterior	540	528.2	0.978
	Left Posterior	545	534.2	0.980

Table 3.2. Point dose comparisons between the treatment planning system and TLD for passive scattering

All of the TLD measured doses were less than calculated for both positions in each irradiation trial, ranging from 1.8% - 3.5%. Our TLD results are found to be within ±4% of calculated values. This is within our acceptable criteria of 5% tolerance for dose agreement.

The reproducibility of the phantom measurements was computed by calculating the coefficient of variance (COV) between point measurements in the target. This was done using the average measured doses from the three trials for each TLD location and can be seen in Table 3.3.

Passive Scattering Doses		
TLD Location	Right Anterior	Left Posterior
Calculated Dose [cGy]	540	545
Measured Dose Avg. [cGy]	525.6	532.4
COV	0.78%	0.75%
Measured/Calculated Dose	0.973	0.977

Table 3.3. Average of measured TLD doses from passive scattering beams for three trials

The COVs for each TLD location both measure less than 0.8%, well under our 3% reproducibility criteria. The small disparity between trial measurements show that we were able to set up the phantom in a reproducible fashion and that it meets the RPC phantom irradiation standard. These results are comparable to those mentioned in Section 2.3.4.3, as found in the phantom study by Molineu *et al*., where photon phantom measurements were found to have 4% accuracy between various institutions. With such a small coefficient of variation, it may be that the lower TLD measured doses were caused by a systematic error due to a shift in the phantom positioning that may have been caused by a loose leveling screw that could have moved one or both of the TLD into a lower dose region. This type of small positioning error would have been hard to detect with on board imaging.

3.3.2 2D Dose Distribution Analysis

The two-dimensional dose distributions were analyzed by comparing the treatment planning dose clouds to the reconstructed dose profiles obtained from the phantom films in the coronal and sagittal planes. The film and CT registrations were achieved with an RMS < 1 mm for all trials, with the RMS Error ranging from 0.13-0.8672 mm for the film, and an RMS 3D ranging from 0.75-0.9 mm for the CT images. A 2D analysis was performed on the data, using the pass criteria of ±5%/3mm and ±5%/5mm. The gamma analyses for passive scattering trial 1 in the sagittal plane are shown below in Figure 3.4.

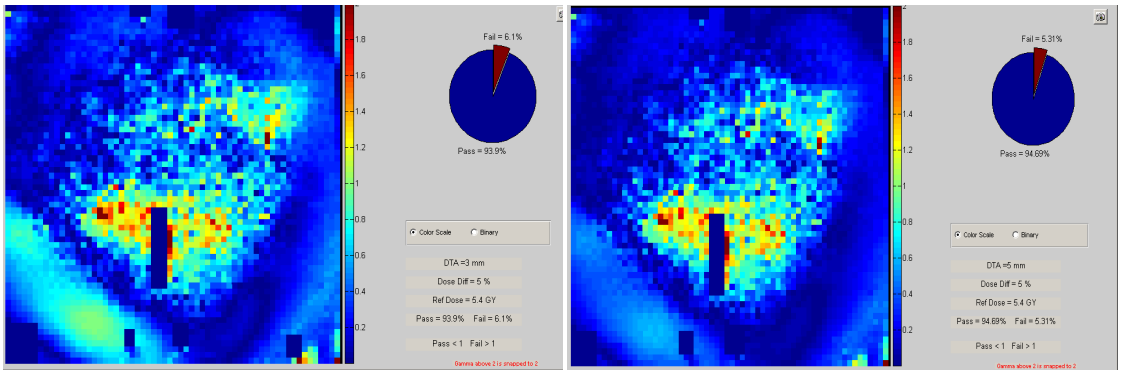

a. **b.**

Figure 3.4. Passive scattering trial 1 sagittal gamma analysis (a. 5%/3mm, b. 5%/5mm)

The complete gamma analysis results for the passive scattering plan are listed in Table 3.4.

Passive Scattering 2D Gamma Percentage of Pixels Passing			
		5%, 3mm	5%, 5mm
Trial 1	Coronal	91.50	98.74
	Sagittal	93.90	94.69
Trial 2	Coronal	91.28	97.63
	Sagittal	91.85	98.62
Trial 3	Coronal	88.00	96.26
	Sagittal	94.86	98.61

Table 3.4. The gamma analysis pass rates for the passive scattering irradiations

Using the pixel pass rate of 85% that the RPC uses, each trial passed both the 5%/5mm and the stricter 5%/3mm gamma analyses. With the range uncertainties associated with proton irradiations, we expect to see some shifts in dosimetric dose profiles when compared with treatment planning dose clouds. As expected, the pass rates were greater for the 5%/5mm criteria, as it allows for a greater distance disagreement in pixel shifts. Overall, the sagittal films showed better pass rates than the coronal films. This is not too surprising, as two separate pieces of film were used in the coronal plane, while one solid piece was used in the sagittal plane. The left and right coronal films were not consistently cut from the same region of the EBT2 film, which may have caused some variability in dose response due to the slight variations in film composition over the

profile of the film. If the experiment were to be repeated, it would be done so with the coronal films cut from adjacent regions of the larger sheets of film.

Despite shortcomings of the experimental design, the pass results of the gamma analysis are in agreement with other studies that verify dosimetry with measurements, such as a patient-specific QA study by Arjomandy *et al*. that yielded similarly high pass percentages (47).

3.3.3 Distance to Agreement

For the passive scattering trial irradiations, the distance to agreement (DTA) values were measured between the treatment planning system and the dose profiles collected from the scanned films. The average distance to agreement from the three irradiation trials are listed in Table 3.5. Often, DTAs are presented in overall shifts in a particular plane, such as 0.5 mm superior. However, as evident in Table 3.5 for the S-I and A-P directions, the shifts did not all occur in a unilateral direction, and the shifts in the L-R directions were much greater on the right side than the left.

Passive Scattering Distance to Agreement Shifts		
	Average DTA [mm]	Std Deviation [mm]
Left	0.6	0.6
Right	3.7	0.4
Inferior	-1.1	0.6
Superior	0.6	0.7
Posterior	-0.8	0.5
Anterior	0.8	0.8

Table 3.5. Distance to agreement measurements between the dose distribution from treatment planning system and from film measured for passive scattering proton beams

For these calculations, a regression fit was calculated for the falloff regions of both the planning system and film profiles. Due to the relatively small size of the film pieces, the regression lines were calculated over varying ranges of the dose falloffs, always starting at the 80% dose point, but ending anywhere from the 65% dose point to the 30% point. The values for each profile were kept consistent for all film trials. The right-left profile of the coronal films is shown in Figure 3.5 with corresponding distance to agreement measurements.

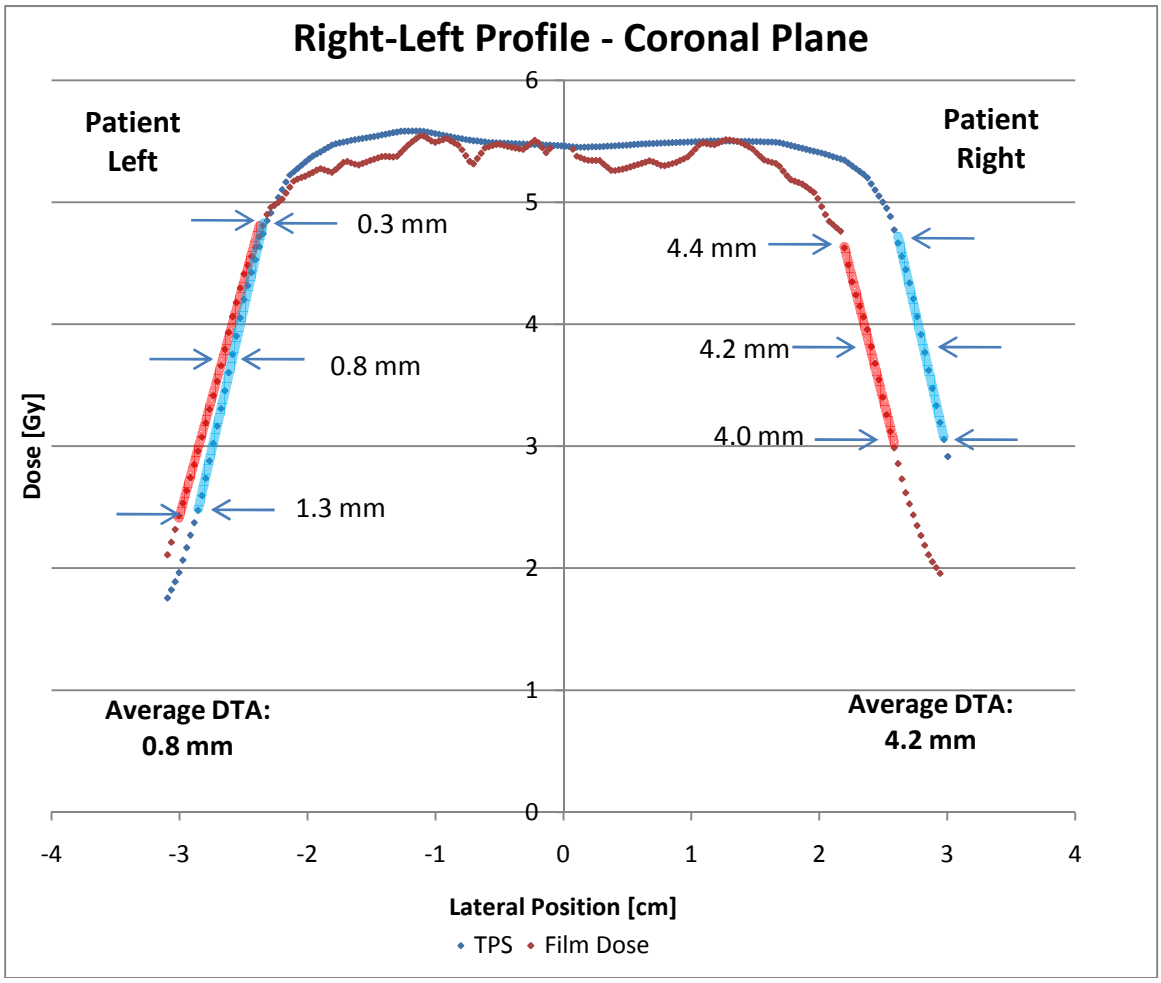

Figure 3.5. Passive scattering trial 1 right-left dose profile DTAs, measured in the coronal plane

As shown above in the L-R direction, there was a much greater shift observed on the right side of the profile than the left side. This calculation is confirmed by the gamma analysis in the coronal plane, where we see more pixels failing the 3mm criteria on the right side of the film than the 5mm criteria, as shown in Figure 3.6.

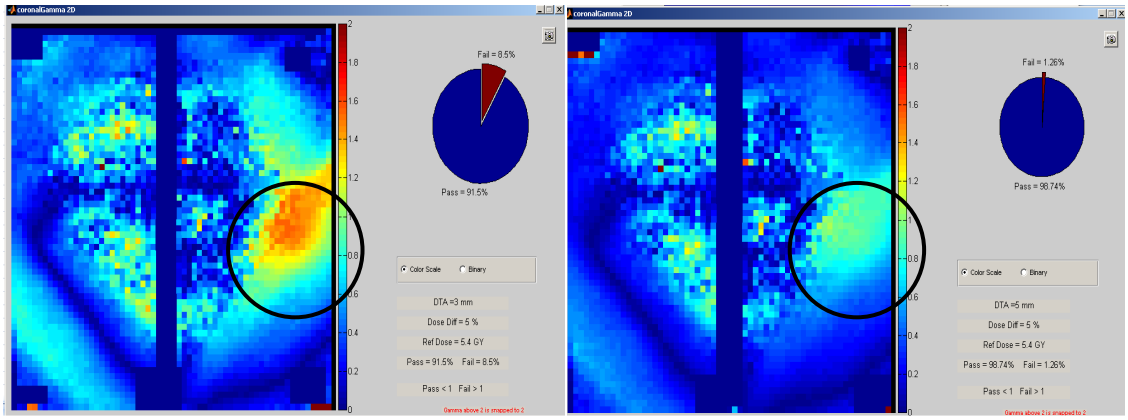

a. **b.**

Figure 3.6. Passive scattering trial 1 coronal gamma analysis (a. 5%/3mm, b. 5%/5mm) with areas of greatest disagreement circled

One set of coronal films was rescanned with adjusted alignment, but this realignment did not produce any improvement in the distance to agreement or pixel pass rates of the trial, which suggest the error in agreement originates in the actual amount of radiation dose delivered. However the error also could have derived from an inconsistency in the physical composition of the two adjacent pieces of film, or poor spatial registration of the film marks.

This was not the case in the S-I shifts – as there was a relatively uniform contraction inward from the treatment plan dose profiles to the film, as delineated in Figure 3.7. The DTA measurements were taken from the 80% to 30% dose points on the inferior side, and the 80% to 65% dose points on the superior side.

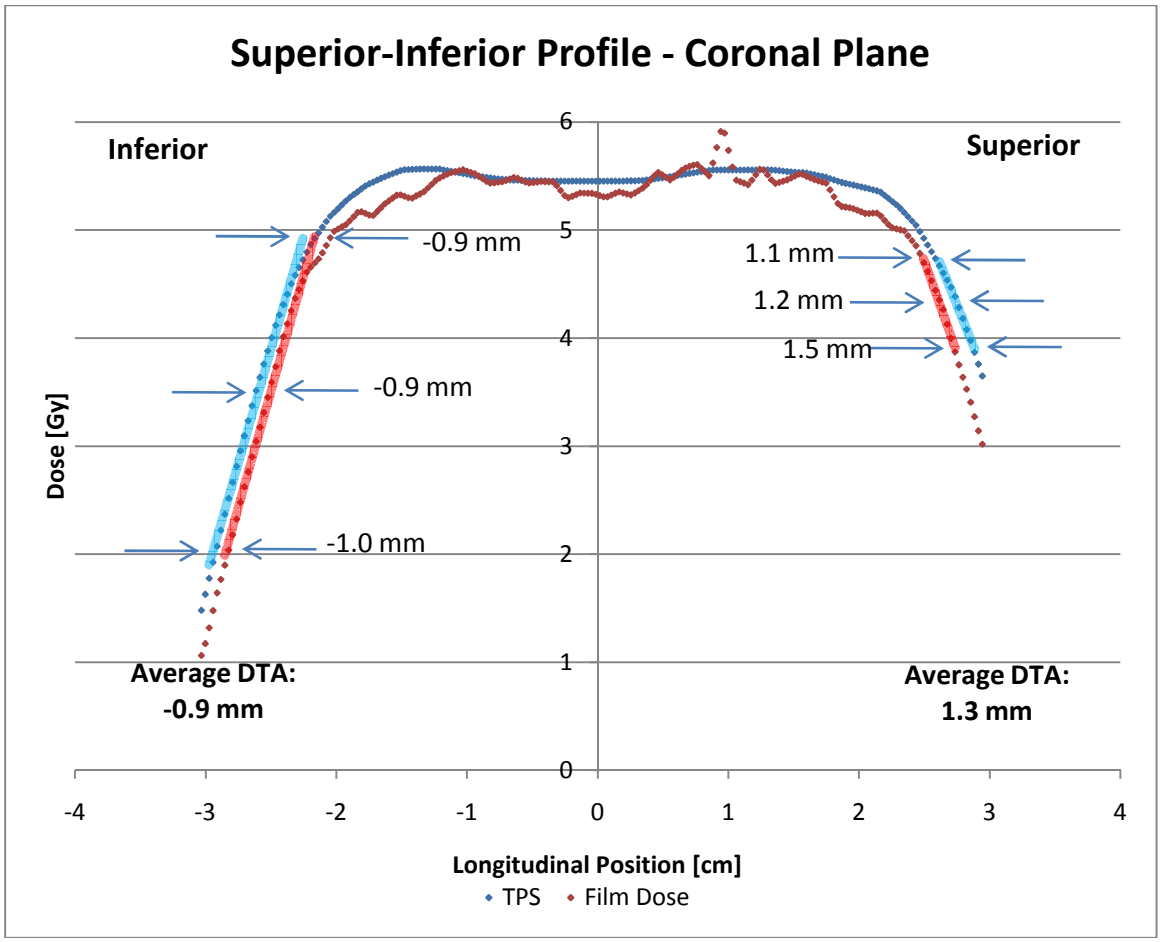

Figure 3.7. Passive scattering trail 1 S-I dose profile DTAs, measured in the coronal plane

As shown above, the S-I DTAs do not suggest an overall shift of the phantom, but rather that the dose delivered does not reach the full S-I extent that the treatment plan predicts. The shifts are small, however, and well within the acceptable tolerance limits of 3mm. In Figure 3.7 it may also be the case that we observe the underresponse of film in the distal edges, which would agree with previous studies that show a film underresponse in the distal edge of the SOBP that may be attributable to an LET dependence of the film that results in higher recombination in the distal edge that prevents the film from polymerizing (43, 46, 48).

In the A-P direction, we saw similar DTA trends as the S-I profiles. Results from Trial 1 are shown in Figure 3.8. The DTAs were calculated using the 80% to 65% dose points on the posterior side, and the 80% to 40% dose points on the anterior side.

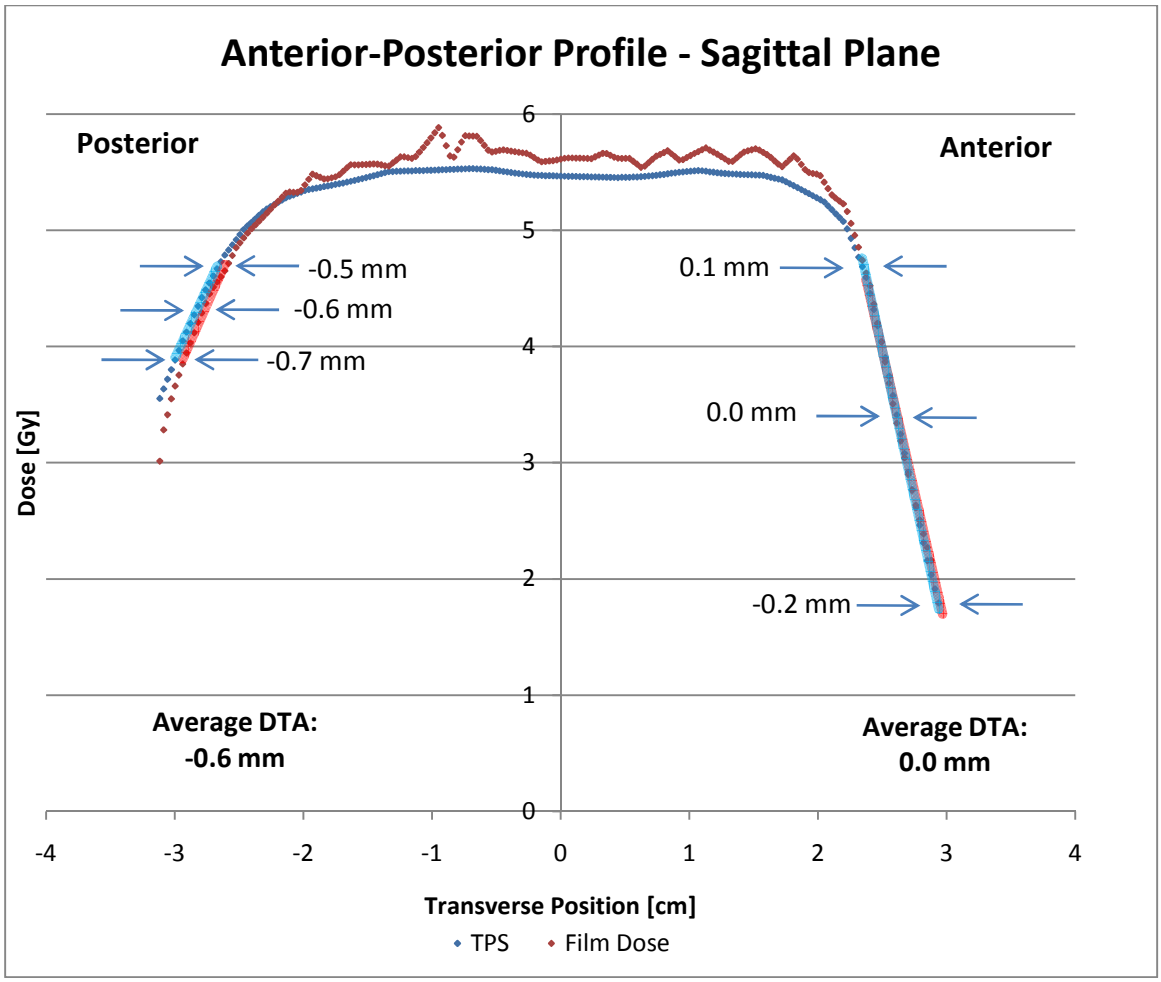

Figure 3.8. Passive scattering trial 1 anterior-posterior dose profile DTAs, measured in the sagittal plane

For the A-P shifts, we see minimal average DTAs that are well within the acceptable 3mm tolerance limits for each passive scattering trial.

3.4 Spot Scanning Phantom Dose Measurements

3.4.1 Absolute Dose Comparison

For an absolute dose comparison, the TLD doses as predicted in the treatment planning system were compared to the measured dose from the TLD capsules in each trial. The ratio of measured to calculated dose is also calculated in Table 3.6. Both capsules were expected to receive 490 cGy.

	Spot Scan			
	TLD Location	Calculated Dose [cGy] - TPS	Measured Dose [cGy] - TLD	Meas./Calc. Dose
Trial 1	Right Anterior	490	490.7	1.001
	Left Posterior	490	489.8	1.000
Trial 2	Right Anterior	490	489.3	0.999
	Left Posterior	490	490.6	1.001
Trial 3	Right Anterior	490	489.7	0.999
	Left Posterior	490	494.9	1.010

Table 3.6. Point dose comparisons between the treatment planning system and TLD for spot scanning

The data demonstrate excellent agreement between the treatment planning system and the TLD measurements for the spot scanning proton beam treatment plans, with a maximum difference of only 1%. These numbers are well within the typical uncertainty of TLD and within the criteria of acceptability. The agreement between measured and calculated values is comparable to those found by Zhu *et al.* when verifying patient specific treatment planning calculations with measured point doses (26).

The reproducibility, as with the passive scattering plan, was calculated by computing the COV of the average TLD measurements for each location. The reproducibility is summarized in Table 3.7.

Spot Scanning		
TLD Location	Right Anterior	Left Posterior
Calculated Dose [cGy]	490	490
Measured Dose Avg. [cGy]	489.9	491.8
COV	0.15%	0.56%
Measured/Calculated Dose	1.000	1.004

Table 3.7. Average spot scanning dose over three trials

The COV for each TLD position was less than 0.6%, which is well under the 3% reproducibility criterion. This indicates that the setup for the spot scanning trial irradiations was reproducible, and could be recreated for the purpose of future audits.

3.4.2 2D Dose Distribution Analysis

As with the passive scattering treatment plan, the two-dimensional dose distribution was analyzed by comparing the dose clouds from the treatment planning system with the dose profiles from the films in the phantom. Film and CT registrations were all achieved with RMS < 1 mm, with the RMS Error ranging from 0.2553-0.7177 mm for film, and a 3D RMS of 0.68 for the CT images (the CT point registration was used for all trials). The gamma analyses for the sagittal plane of trial 1 of the spot scanning plan is shown below in and the complete 2D gamma analysis results for each spot scanning trial are listed in Table 3.8.

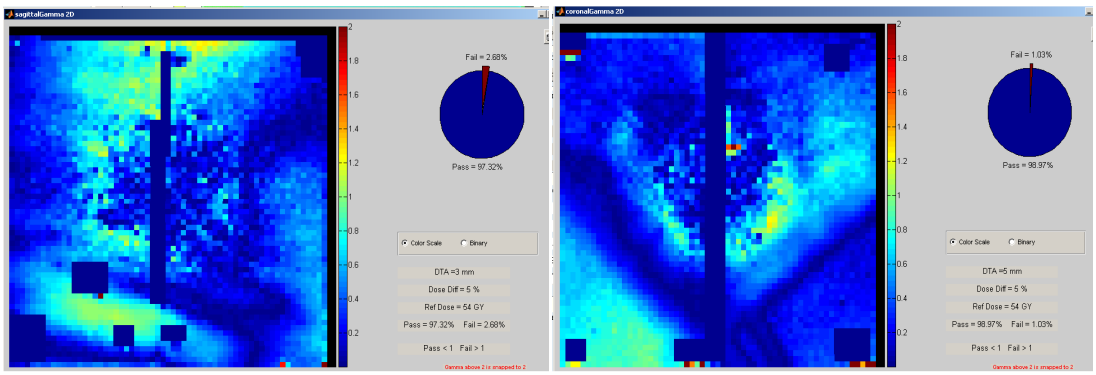

a. **b.**

Figure 3.9. Spot scanning trial 1 sagittal gamma analysis (a. 5%/3mm, b. 5%/5mm)

Spot Scanning Doses 2D Gamma Percentage of Pixels Passing			
		5%, 3mm	5%, 5mm
Trial 1	Coronal	88.12	98.97
	Sagittal	97.32	99.91
Trial 2	Coronal	84.86	98.56
	Sagittal	98.79	99.74
Trial 3	Coronal	80.59	93.56
	Sagittal	92.89	99.74

Table 3.8. 2D gamma analysis pass rates for the spot scanning irradiations

The film passed well with the 5%/5mm criteria. The stricter 5%/3mm criteria were not met as well, with the coronal planes showing poorer pixel pass rates for every trial. However, the combined average pass rates for each trial all exceed the 85% pixel pass rate criteria set forth by the RPC, as shown in Table 3.9.

Spot Scanning 2D Gamma Pass Rate – Per Trial		
	5%, 3mm	5%, 5mm
Trial 1	92.7	99.4
Trial 2	91.8	99.2
Trial 3	86.7	96.7

Table 3.9. 2D gamma pass rates averaged over each trial irradiation

When reviewing the average gamma pass rates for different planes, all show good agreement except the coronal plane for the 5%/3mm criteria, where the pixel pass rate was just under the desired 85%, as delineated in Table 3.10. However, the coronal films had good agreement (97%) under 5%/5mm criteria. This suggests that pixel shift is present between the planned dose distribution and the physical delivery in the coronal plane.

Spot Scanning 2D Gamma Pass Rate		
	5%, 3mm	5%, 5mm
Coronal	84.5	97.0
Sagittal	96.3	99.8
Sum	90.4	98.4

Table 3.10. 2D gamma pass rates averaged by film plane

3.4.3 Distance to Agreement

The treatment planning dose profiles were measured against the film dose profiles to obtain distance to agreement values. As with the passive scattering measurements, the DTAs were determined in the dose falloff regions over varying ranges depending on the doses available on the film. These ranges were kept consistent for all trials, but varied by plane. The average spot scanning DTAs are shown in Table 3.11.

Spot Scanning Distance to Agreement Shifts		
	Average DTA [mm]	Std Deviation [mm]
Left	0.1	0.8
Right	3.4	0.5
Inferior	-1.8	0.9
Superior	2.2	1.7
Posterior	-1.2	0.4
Anterior	0.0	0.5

Table 3.11. Distance to agreement measurements between dose distributions from treatment plans and from film measured for spot scanning proton beams

As with the passive scattering irradiations, we see the greatest disagreement between the treatment planning system prediction and measured film dose profiles in the coronal plane in the L-R direction. The distance to agreement measurements were calculated between the 80% and 50% dose points for both the left and right sides for all trials. This dose profile is shown in Figure 3.10.

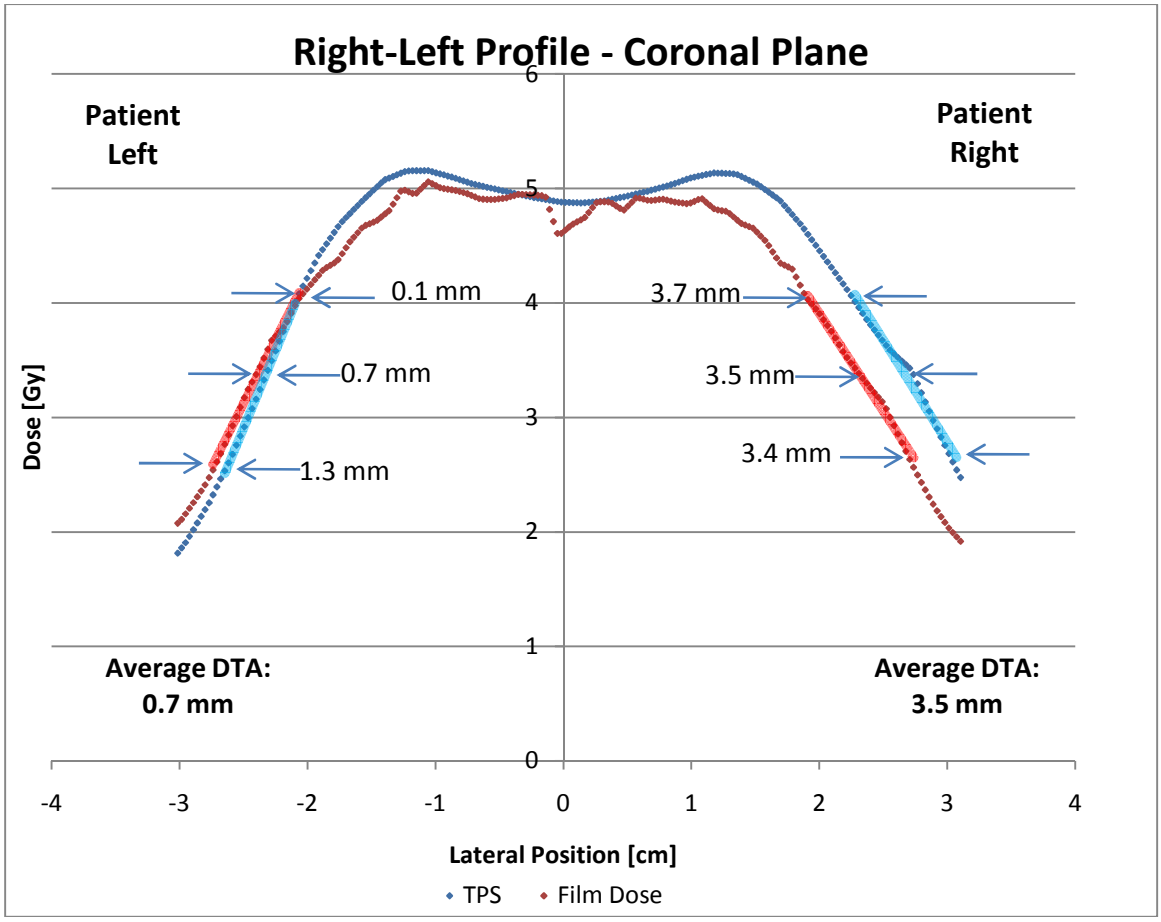

Figure 3.10. Spot scanning trial 1 right-left dose profile DTAs, measured in the coronal plane

The left side of the dose profile shows good agreement between the TPS and film, but the right side has much greater average displacement, with film doses not reaching as far as the treatment planning system predicts. This right side displacement is greater than the 3mm we desire for the stricter criteria, as highlighted in the circled areas of gamma

analysis failure in Figure 3.11. However when we look at these same regions of interest within the looser 5mm standards, the gamma analysis shows better agreement.

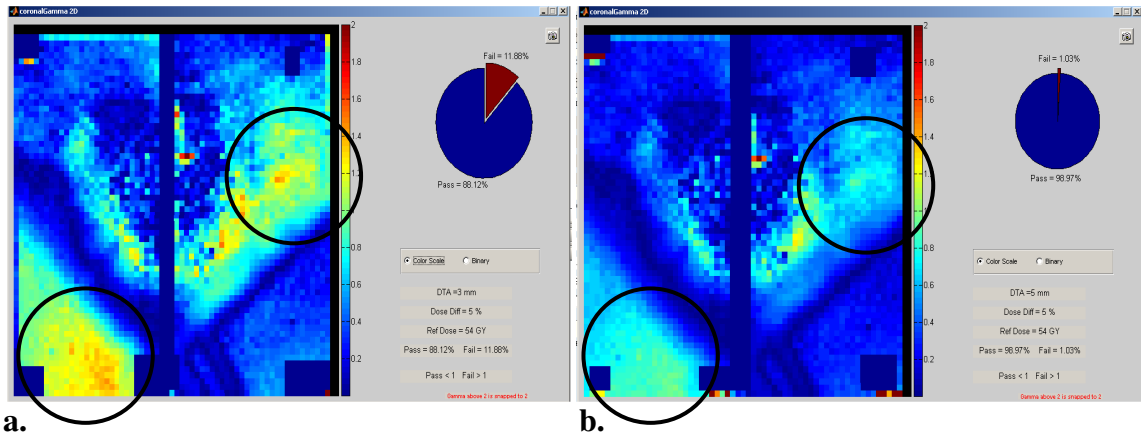

a. **b.**

Figure 3.11. Spot scanning trial 1 coronal gamma analysis with areas of disagreement highlighted (a. 5%/3mm, b. 5%/5mm)

The disagreement highlighted in Figure 3.11is present in all of the right-left gamma analyses for each of the three spot scanning trials. The disagreement in the lower left corner of the film is most concerning, as this indicates dose to a region outside of the target. We suspect a small shift is responsible for this disagreement (and thus the disagreement is not seen on the loser 5%/5mm criteria). However the DTA calculations do not reflect this disagreement in the right-left profile due to the positioning of the DTA profile across the center of the piece of film. Taking this into account, it might be advantageous to run a profile and DTA measurements across a more inferior portion of the film plane. This would give us a more quantifiable shift calculation for the dose to the region of normal tissue.

As with the passive scattering trials, the S-I DTAs suggest the film doses were delivered over a narrower extent than the treatment planning dose profiles, as shown below in Figure 3.12. The DTAs were measured from the 80% to 30% dose points on the inferior side, and the 80% to 50% dose points on the superior side. While the inferior DTA is consistently greater than the superior side, both shifts are within the 3 mm criteria.

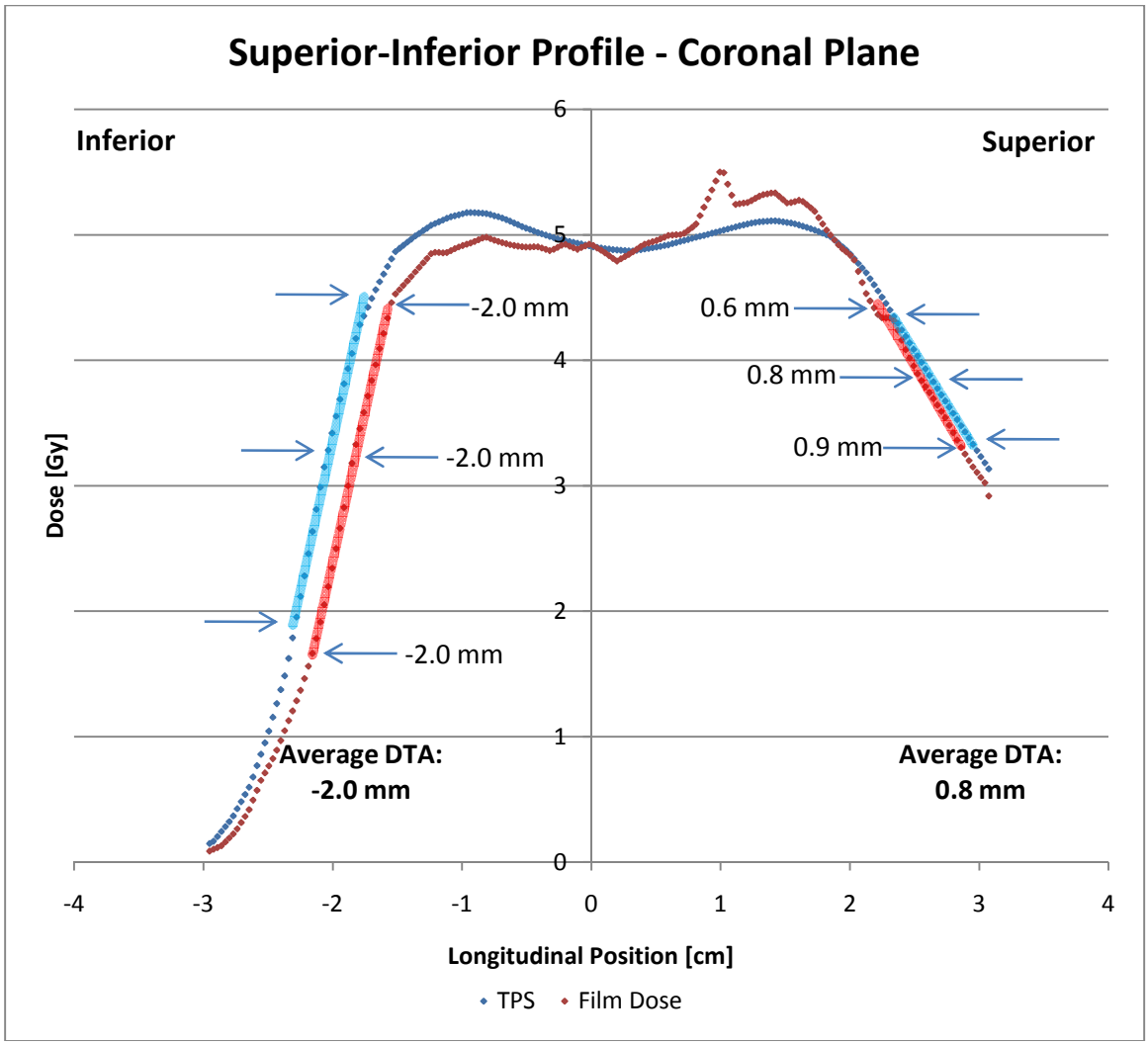

Figure 3.12. Spot scanning trial 1 S-I dose profile DTAs, measured in the coronal plane

The anterior-posterior dose profiles showed minimal shift on both the anterior and posterior sides. The DTAs were calculated for the dose point ranges between 80% and 60% on the posterior side, and between 80% and 50% on the anterior side. The Trial 1 profile comparisons are shown in Figure 3.13. The displacement on each side is less than 1.3 mm, well within our 3 mm criteria.

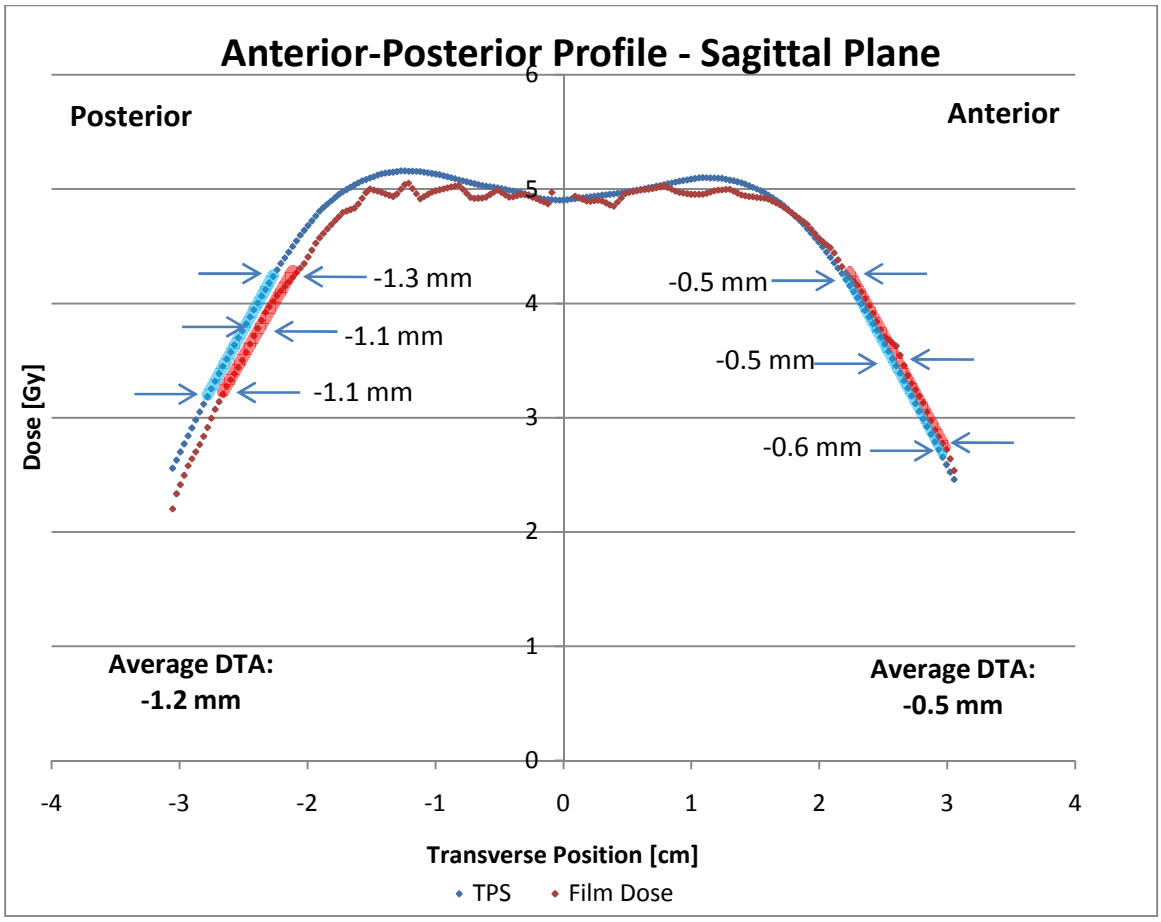

Figure 3.13. Spot scanning trial 1 A-P dose profile DTAs, as measured in the sagittal plane

3.5 Passive Scattering & Spot Scanning Results Comparison

The passive scattering and spot scanning irradiation results are comparable under most criteria, but there are a few areas of distinction worth highlighting. First, though both systems passed the absolute point dose criteria, the passive scattering system showed much greater disagreement (1.8 – 3.5%) than the spot scanning system (<1%). However, in a previous study conducted at the PTC-H by Zullo *et al.*, TLD-100 was found to predict dose within ±5% of predicted dose for passively scattered beams, which agrees well with our results (39).

Another area of difference between the passive scattering and spot scanning systems was the gamma analysis in each film plane, as shown in Table 3.12. While the passive scattering system showed good agreement in the coronal plane, the spot scanning system showed poorer agreement in this plane. As discussed above, the lower pass rate of

the spot scanning system in the coronal plane was likely caused by a right-left shift of the phantom or dose delivery, as the spot scanning coronal gamma pass rate increases significantly for the 5%/5mm criteria. However there was not a larger right-left DTA shift observed in the spot scanning system over the passive scattering system. But as mentioned in Section 3.4.3, the DTA measurement is only made over a profile capturing a singular slice of the film plane, and as such may misrepresent the DTA over the entire film plane.

2D Gamma Percentage of Pixels Passing 5%, 3mm Criteria			
		Passive Scattering	Spot Scanning
Trial 1	Coronal	91.50	88.12
	Sagittal	93.90	97.32
Trial 2	Coronal	91.28	84.86
	Sagittal	91.85	98.79
Trial 3	Coronal	88.00	80.59
	Sagittal	94.86	92.89

Table 3.12. 2D gamma analysis pixel pass rates for 5%/3mm criteria

Lastly, continuing the discussion of distance to agreement measurements, the passive scattering and spot scanning systems demonstrated comparable DTAs in every direction except the superior direction; the passive scattering irradiations showed a superior DTA of 0.6 mm, while the spot scanning irradiations had an average DTA of 2.2 mm. These shifts are both within the limits set, but there may have been a greater error in positioning of the phantom during the spot scanning irradiations that contributed to a larger dose disagreement in the superior direction. This likely also contributed to the lower 2D gamma analysis pass rates of the spot scanning films in the coronal plane.

4 Conclusions

4.1 Meeting Specific Aims

This project was designed to create and test a proton therapy head phantom to be used for auditing proton facilities participating in clinical trials. The hypothesis was to see if the treatment procedure could produce measured doses that agreed with calculated doses within 5%/3mm with a reproducibility of 3%.

The first specific aim, to select a head phantom design and find appropriate materials for the phantom construction, was achieved. The design of the phantom allows for easy simulation, especially with the presence of a human skull, which improves image-guided setup. The tissue equivalent phantom materials tested and used – the Alderson material, nylon, high density polyethylene, and acrylic – were all found to lie close to the calibration curve for stopping power and Hounsfield units used in the PTC-H Eclipse treatment planning system. This allowed the phantom to best simulate human anatomy for the target site.

As the phantom materials were developed with the treatment process in mind, we were able to successfully simulate the phantom using MR and CT, with the appropriate phantom materials showing up well on the imaging modalities. The MR simulation was time consuming, which was not preferable, but the image quality was well suited for target delineation when the image set was fused with the CT images. Treatment plans for both the passive scattering and spot scanning systems were created that both met the modified dose constraints of the clinical trial under consideration and met the department standards at the PTC-H, as verified by a staff physician. The phantom was irradiated without problem on both the passive scattering and spot scanning proton beams at the PTC-H, completing the work described in specific aim two.

Specific aim three was achieved when the point doses and dose distributions for each trial of each irradiation were measured by TLD and film, respectively. When performing the film calibration, it was discussed whether or not to include the 7.5 Gy data points when calculating the optical density relation. This would have made the 5.5 Gy data point the last in the series. Since the high treatment doses expected were around

5.4 Gy, and some “hot” spots were anticipated, it was decided that including the 7.5 Gy data point was appropriate to get a better polynomial fit over the range of doses.

Research work for specific aim four was completed by comparing the film and TLD results from the trial irradiations to the corresponding quantities calculated by the treatment planning system. The deviations and precision of the point doses and 2D dose calculations were measured and analyzed, and showed acceptable results according to our pass rate criteria set for the phantom, with an average of 91.9% of passive scattering pixels and 90.4% of spot scanning pixels passing 5%/3mm gamma analysis criteria, with a reproducibility within 0.8% for the passive scattering system and within 0.6% for the spot scanning system.

There were some limitations in the accuracy of our data associated with specific aim four. When performing the gamma analyses for the dose distribution comparisons, the passive scattering analysis did not utilize the same CT registration for all trials, due to difficulties with the MATLAB software. This produced a range of 3D RMS errors for the CT registration, which may have contributed to overall uncertainty in the gamma analysis. If the project were to be repeated, the same CT registration would be used for all irradiation trials.

The greatest area of concern with the distance to agreement shifts observed between film and treatment planning profiles is the large shift observed on the right side of the coronal films. It is unexpected that the right side shift should disagree so much with the left side, and for that reason it needs to be reinvestigated more carefully. One possible explanation of this disagreement is a rotation in the setup of the phantom head before irradiation. It is possible that one of the leveling screws was bumped from the original simulation position, which could have caused a minimal shift on one side of the profile and a greater disagreement on the other side. If this is the case, simply adjusting the resistance of the leveling screws, or creating a way of marking their level, could help prevent future misalignment.

The distance to agreement measurements in the S-I and A-P directions were minimal and agree well with the predictions from the treatment planning system, within our 3 mm criterion.

It seems that the passive scattering plans demonstrate strong overall alignment, with the pixel pass rate not changing much between the 5%/3mm and 5%/5mm criteria, while the spot scanning treatment plans seem to show a shift disagreement, but better overall dose agreement between the treatment plan and dosimetric measurements. Perhaps these results can help the proton community better analyze the uncertainties associated with phantom measurements for both the passive scattering and spot scanning treatment delivery systems.

The hypothesis of this project was that an anthropomorphic head phantom could be developed to evaluate proton therapy patient simulation, treatment planning, and treatment delivery to assure agreement between the measured dose and calculated dose within ±5%/3mm with a reproducibility of ±3%. With over 90% 5%/3mm agreement for both the passive scattering and spot scanning systems, and a reproducibility within 0.8% for both systems, the experiments support the hypothesis that a head phantom suitable for the evaluation of proton therapy can be created and commissioned to meet the agreement and reproducibility standards.

4.2 Clinical Significance

As previously discussed, there is a need to verify the proton therapy treatment procedures for institutions participating in relevant clinical trials. With the phantom measurements of dose distribution showing good agreement with those from the treatment planning system, it can be used as a benchmark for facilities wishing to enter proton therapy clinical trials involving the treatment of brain tumors. The RPC would require that a proton therapy facility successfully complete the phantom irradiation audit procedure either before they treated patients on the clinical trial protocol or before a certain number of patients was treated. This standard of credentialing would help ensure that all proton therapy institutions are performing to the same high standards in order to ensure excellent patient care and clinically viable research trial results. This credentialing process not only benefits the patients participating in clinical trials, but also any patient that is subsequently treated on a proton therapy machine that has undergone the RPC phantom quality assurance process.

4.3 Future Directions

Based on the results of the study, it seems appropriate to begin use of the head phantom for the auditing of proton therapy treatment facilities. Initially, the phantom may be used on RPC site visits to participating institutions. If the phantom proves to work well for the site visits, the RPC should be able to incorporate it into the mailable phantom program. This will take some adjustment of current phantom irradiation instructions and procedures.

To further improve upon the phantom design, it might be desirable to add critical structures to the phantom (or a new one like it) to increase the difficulty of the phantom irradiation, as well as collect data on the proton centers' ability to avoid dosing such structures. Another future direction that was discussed throughout the course of the project was adapting the phantom to include a typical Head & Neck target, such as an oropharyngeal or nasopharyngeal tumor volume. The phantom, with its anatomical mimicry of nasal and oral passageways, would be well suited for a realistic experiment of this type. It may prove difficult to properly model human air passages, as a common clinical problem with treatment planning and delivery in such areas is the changing

volume of mucus within these cavities. This could be modeled in the phantom by introducing gel or a gel-filled balloon into the phantom airways, and may be a good way of looking at the discrepancy between the planned v. delivered doses when mucus volume changes. With the addition of any of these modifications, the phantom could be improved from its original design to adapt to the changing needs of proton therapy audits.

5 Appendix

5.1 Gamma Analysis

5.1.1 Passive Scattering Plan

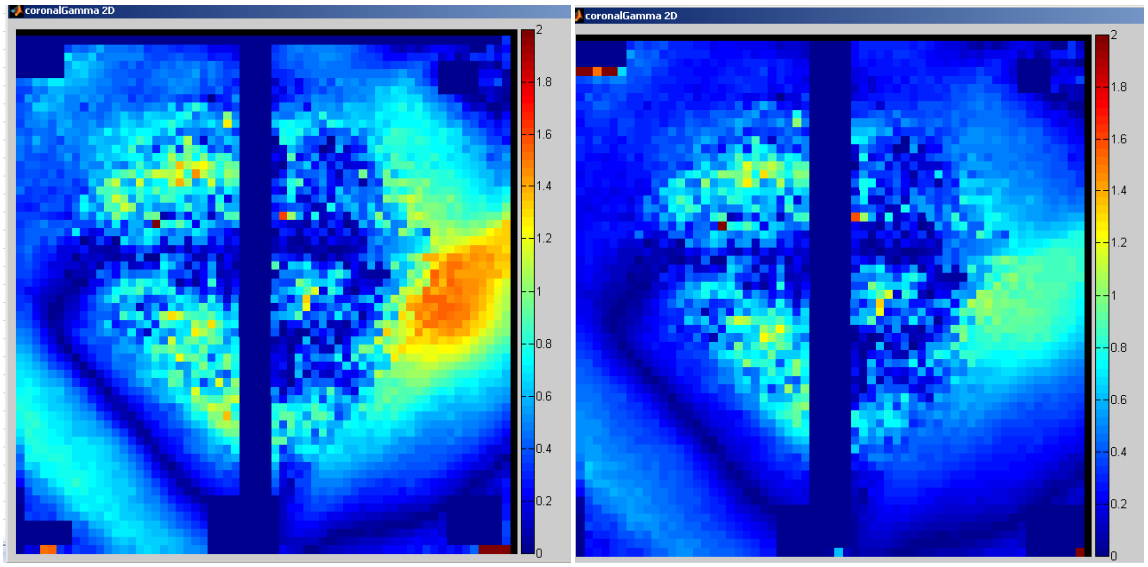

a. 5%/3mm: 91.50% pass **b. 5%/5mm: 98.74% pass**

Figure 5.1. Passive Scattering Trial 1 Coronal Gamma Analyses

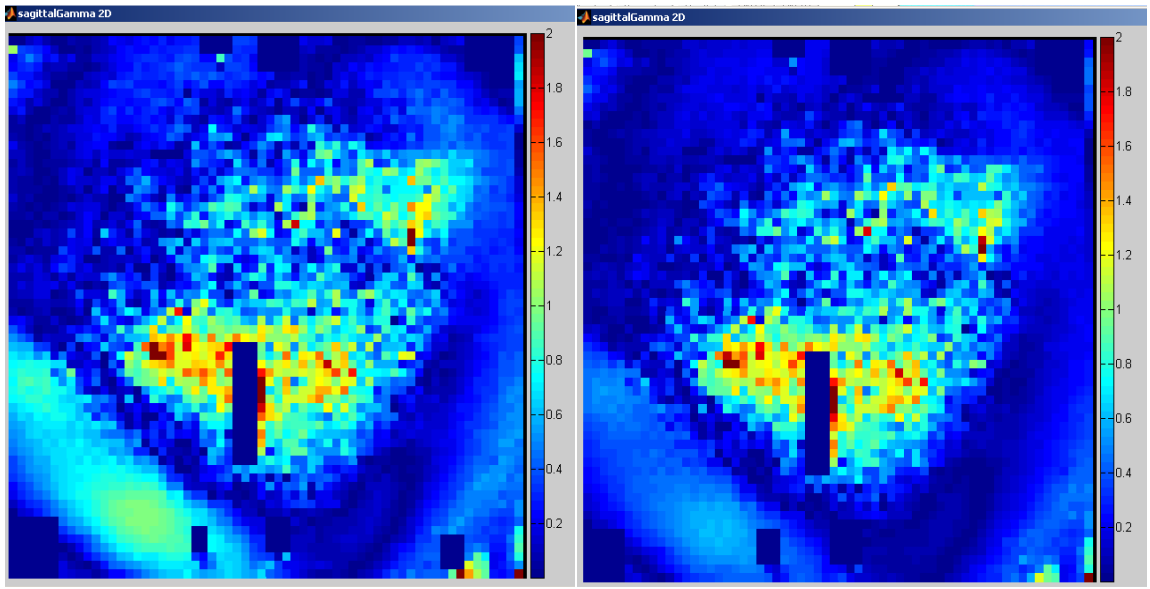

a. 5%/3mm: 93.90% pass **b. 5%/5mm: 94.69% pass**

Figure 5.2. Passive Scattering Trial 1 Sagittal Gamma Analyses

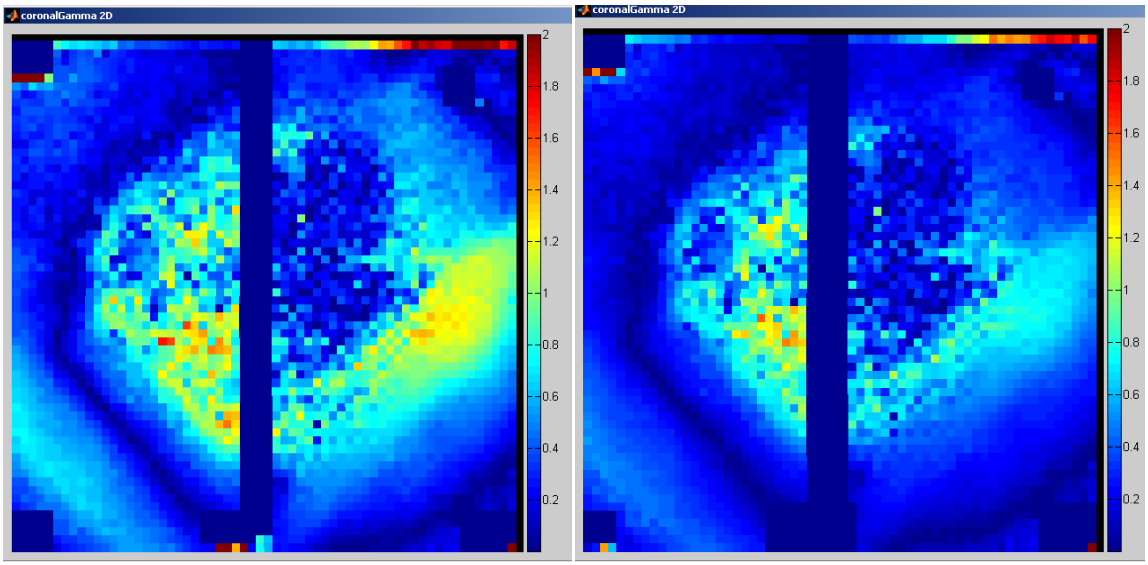

a. 5%/3mm: 91.28% pass **b. 5%/5mm: 97.63% pass**

Figure 5.3. Passive Scattering Trial 2 Coronal Gamma Analyses

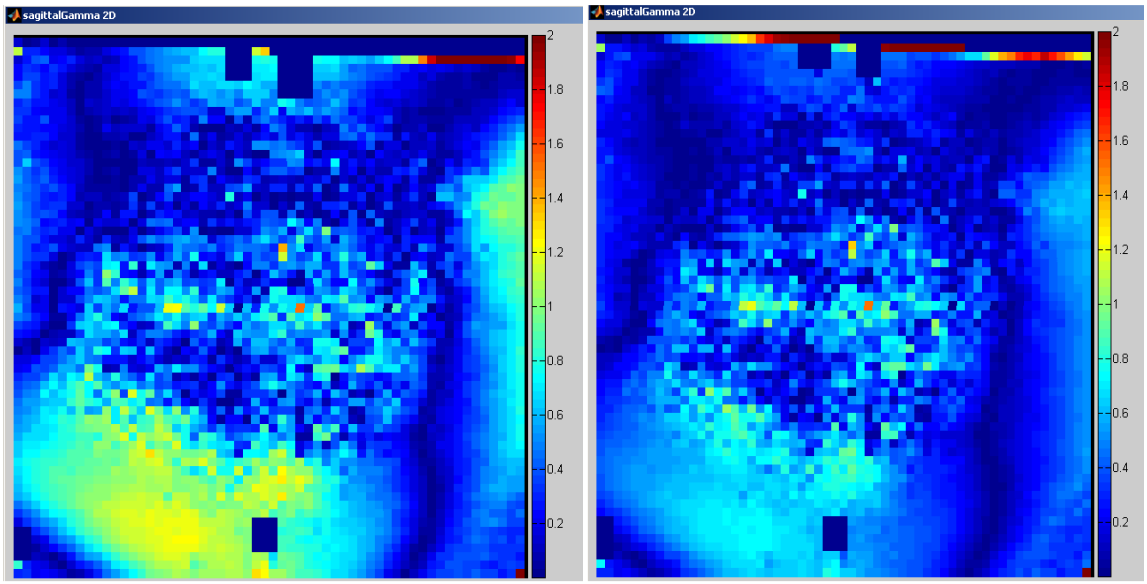

a. 5%/3mm: 91.85% pass **b. 5%/5mm: 98.62% pass**

Figure 5.4. Passive Scattering Trial 2 Sagittal Gamma Analyses

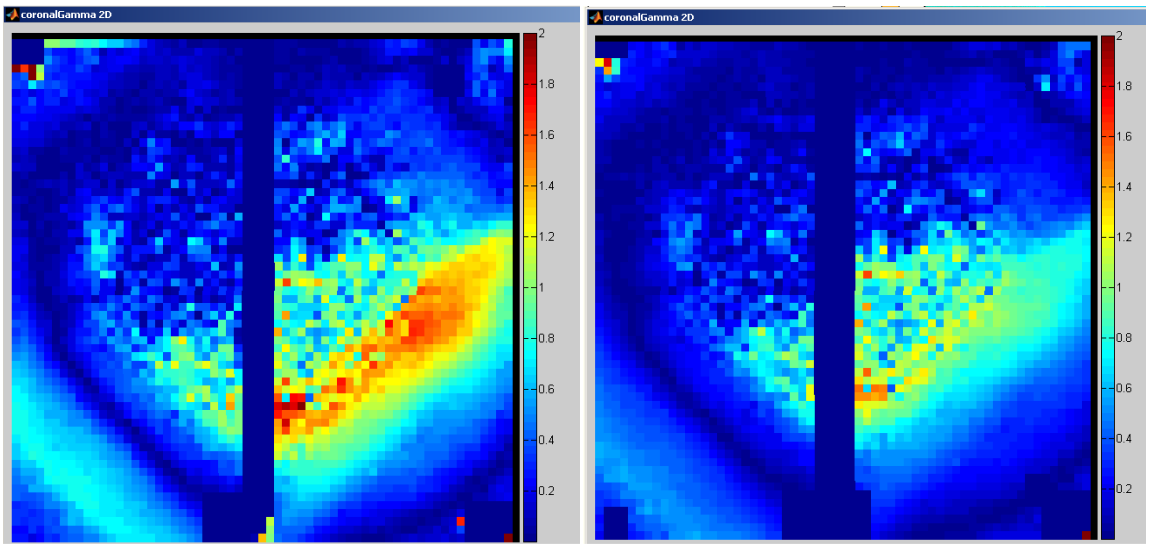

a. 5%/3mm: 88.0% pass **b. 5%/5mm: 96.26% pass**

Figure 5.5. Passive Scattering Trial 3 Coronal Gamma Analyses

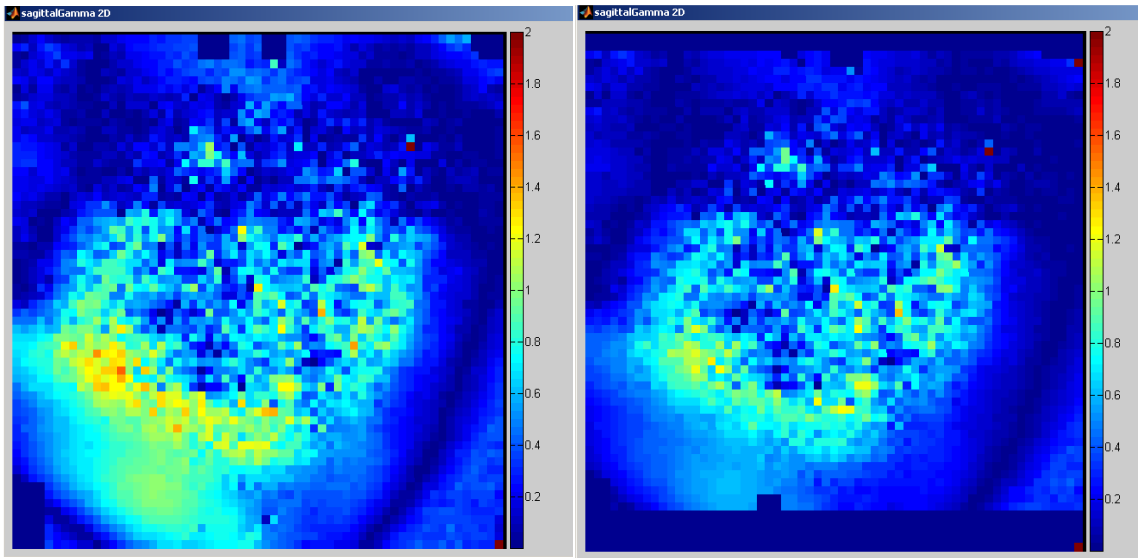

a. 5%/3mm: 94.86% pass **b. 5%/5mm: 98.61% pass**

Figure 5.6. Passive Scattering Trial 3 Sagittal Gamma Analyses

5.1.2 Spot Scanning Plan

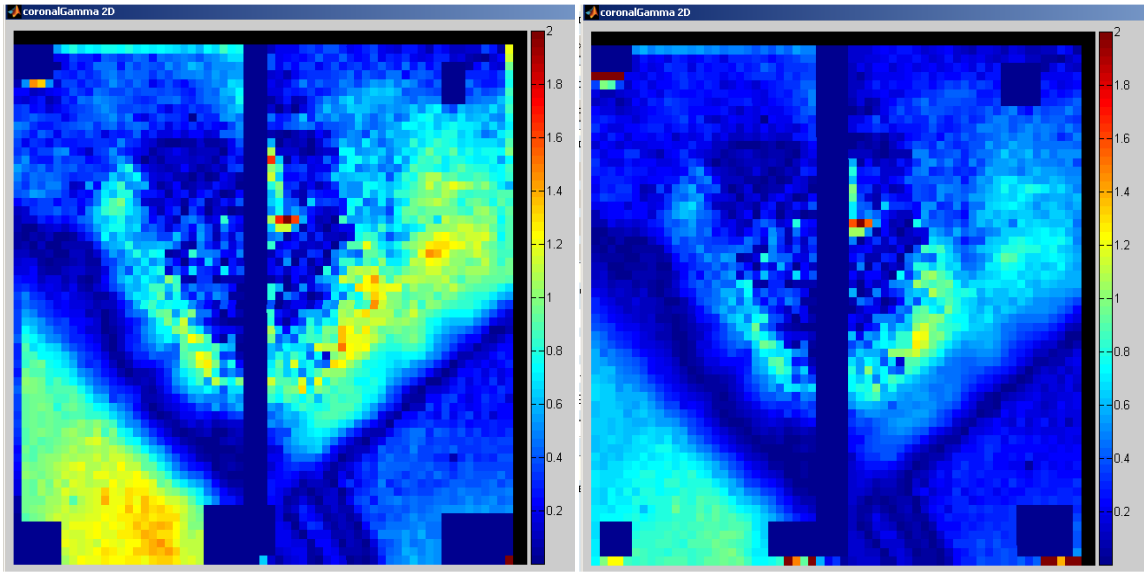

a. 5%/3mm: 88.12% pass **b. 5%/5mm: 98.97% pass**

Figure 5.7. Spot Scanning Trial 1 Coronal Gamma Analyses

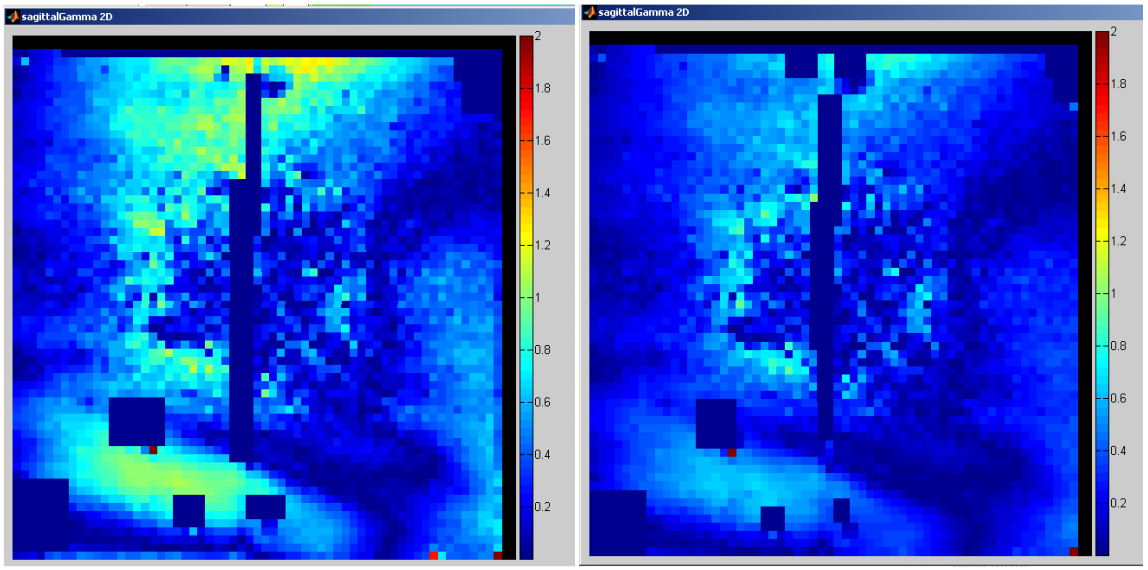

a. 5%/3mm: 97.32% pass **b. 5%/5mm: 99.91% pass**

Figure 5.8. Spot Scanning Trial 1 Sagittal Gamma Analyses

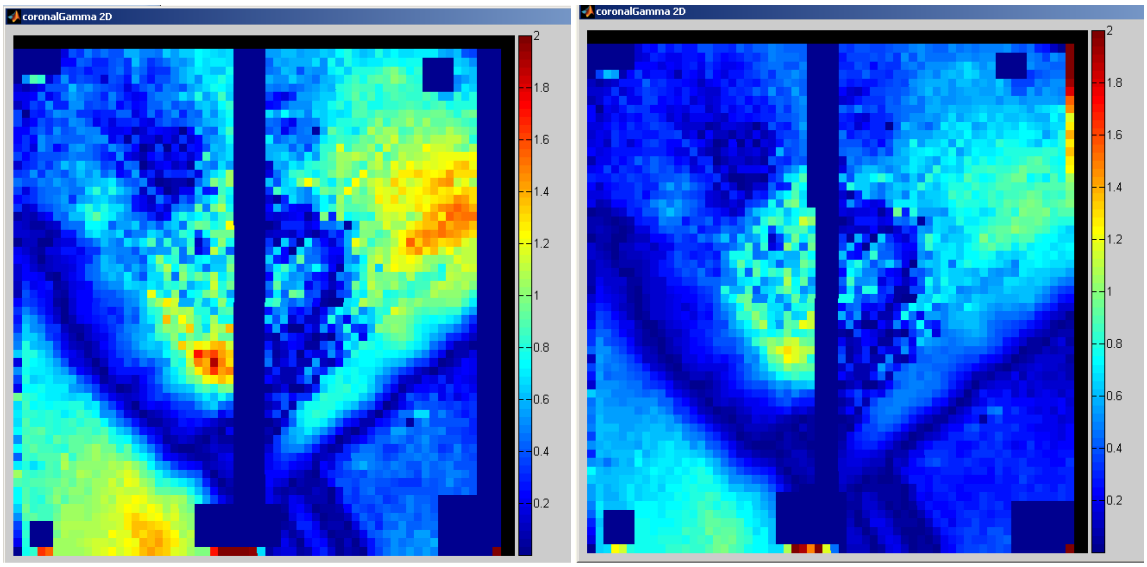

a. 5%/3mm: 84.86% pass **b. 5%/5mm: 98.56% pass**

Figure 5.9. Spot Scanning Trial 2 Coronal Gamma Analyses

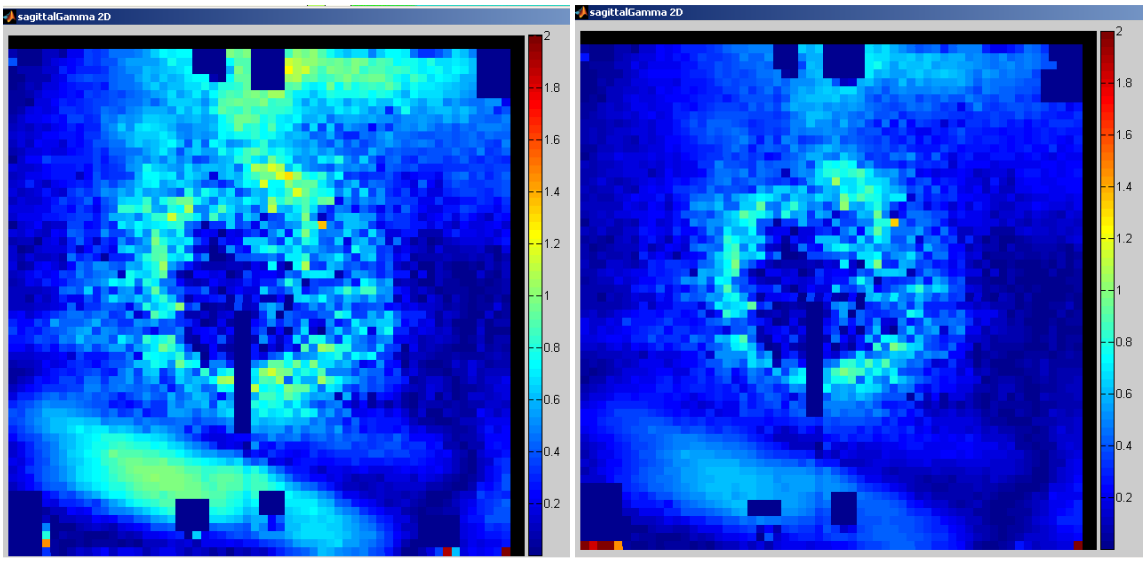

a. 5%/3mm: 98.79% pass **b. 5%/5mm: 99.74% pass**

Figure 5.10. Spot Scanning Trial 2 Sagittal Gamma Analyses

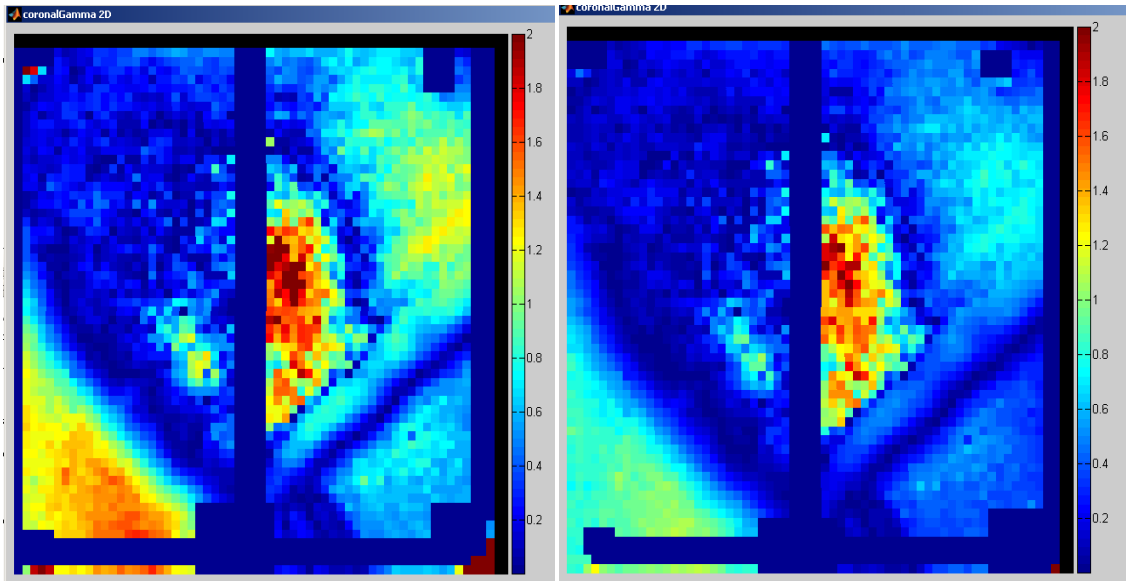

a. 5%/3mm: 80.59% pass **b. 5%/5mm: 93.56% pass**

Figure 5.11. Spot Scanning Trial 3 Coronal Gamma Analyses

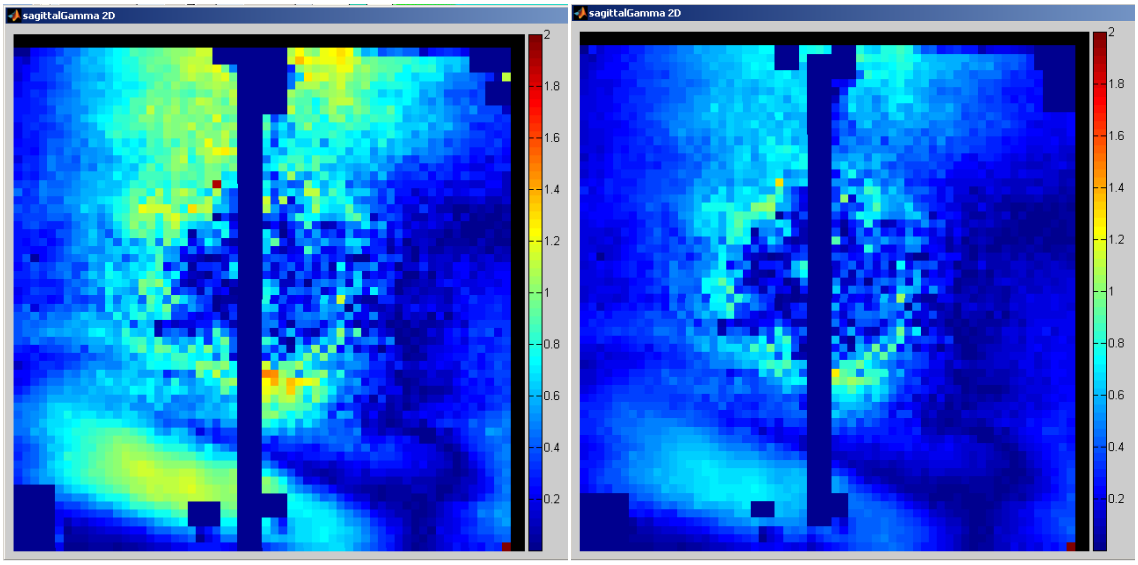

a. 5%/3mm: 92.89% pass **b. 5%/5mm: 99.74% pass**

Figure 5.12. Spot Scanning Trial 3 Sagittal Gamma Analyses

5.2 Dose Profile Comparisons

5.2.1 Passive Scattering Plan

5.2.1.1 Trial 1

See Section 3.3.3 for trial 1 results.

5.2.1.2 Trial 2

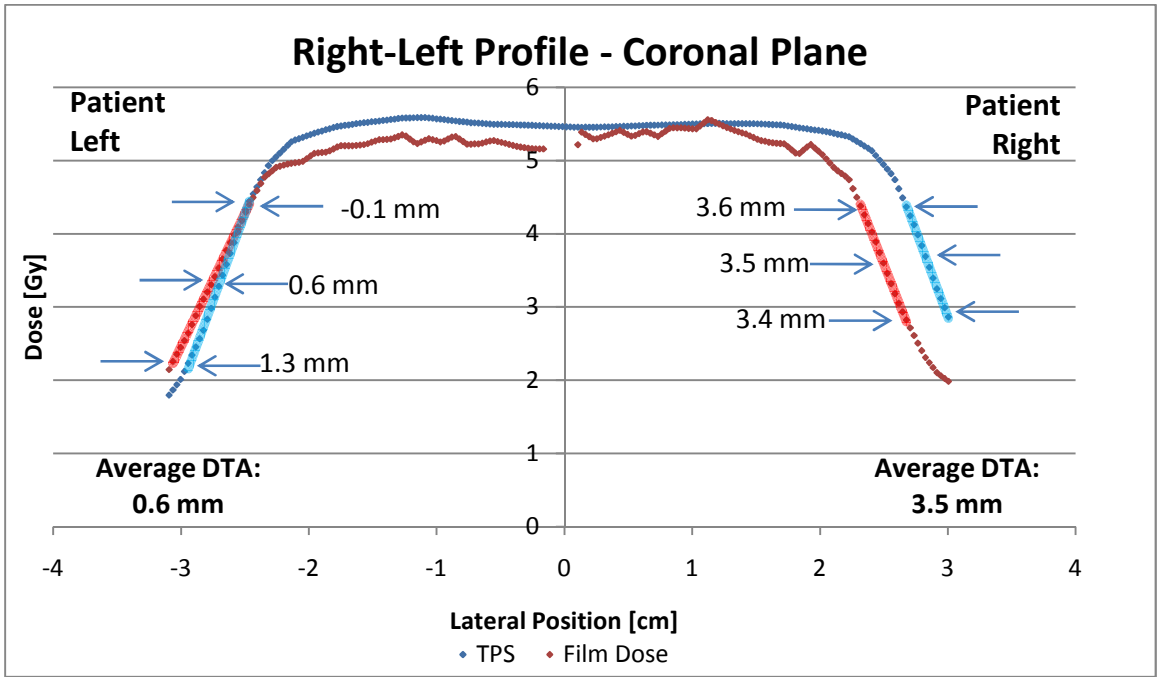

Figure 5.13. Passive scattering trial 2 R-L dose profile DTAs, measured in the coronal plane

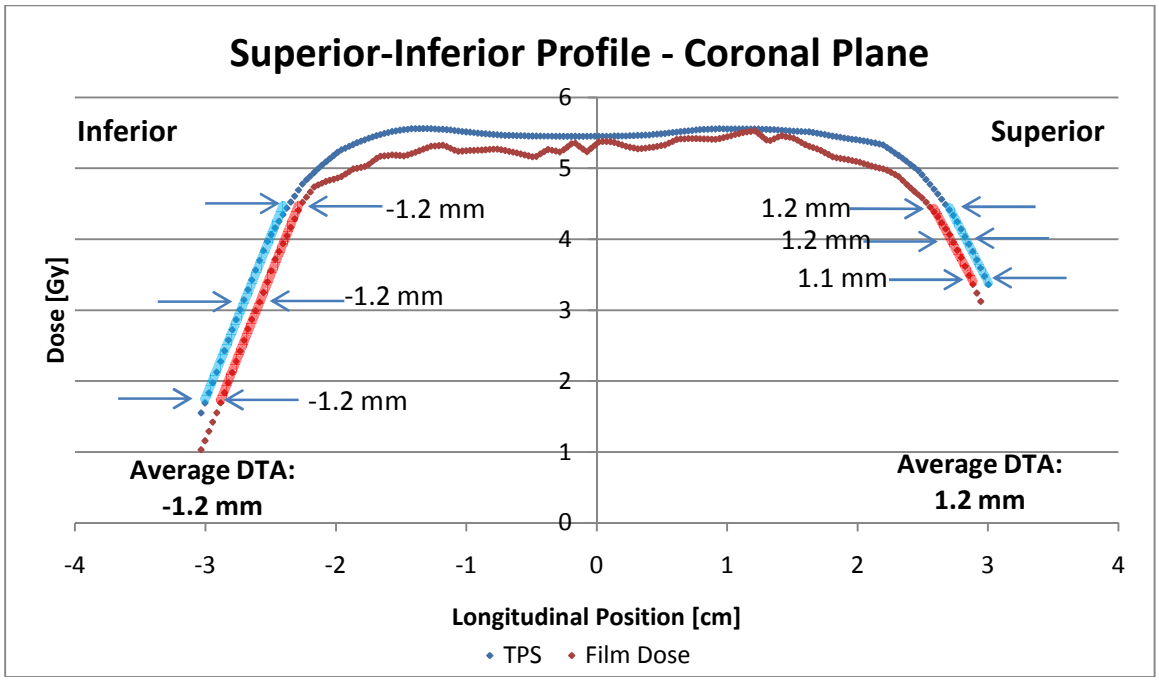

Figure 5.14. Passive scattering trial 2 S-I dose profile DTAs, measured in the coronal plane

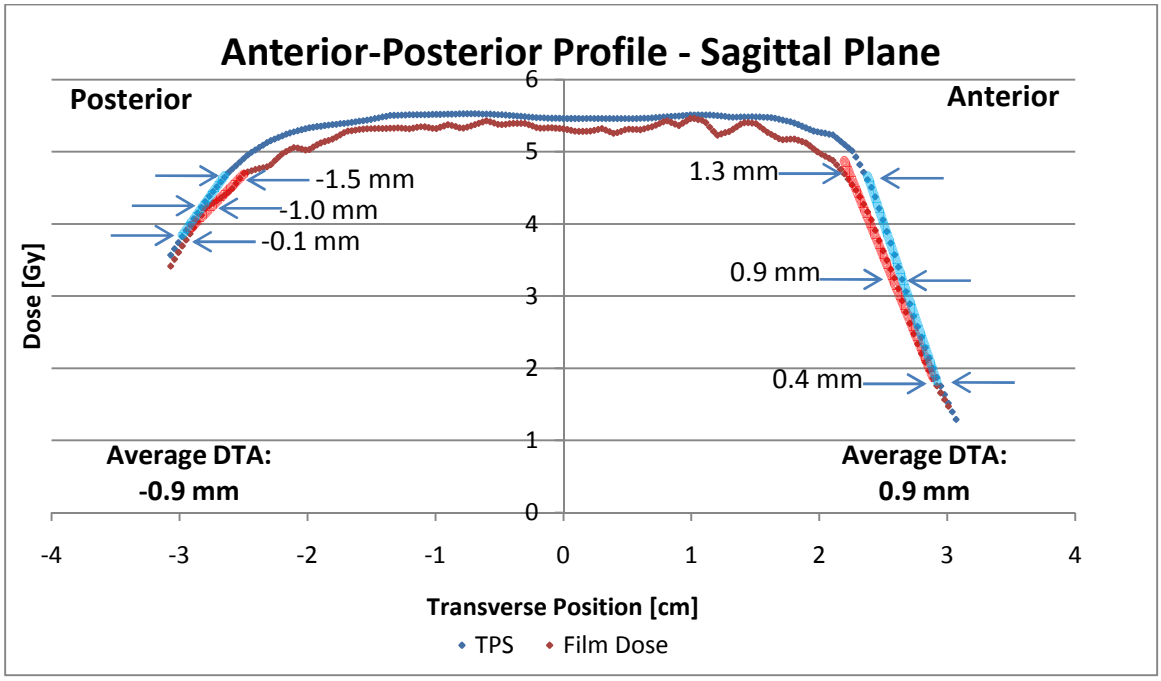

Figure 5.15. Passive scattering trial 2 A-P dose profile DTAs, measured in the sagittal plane

5.2.1.3 Trial 3

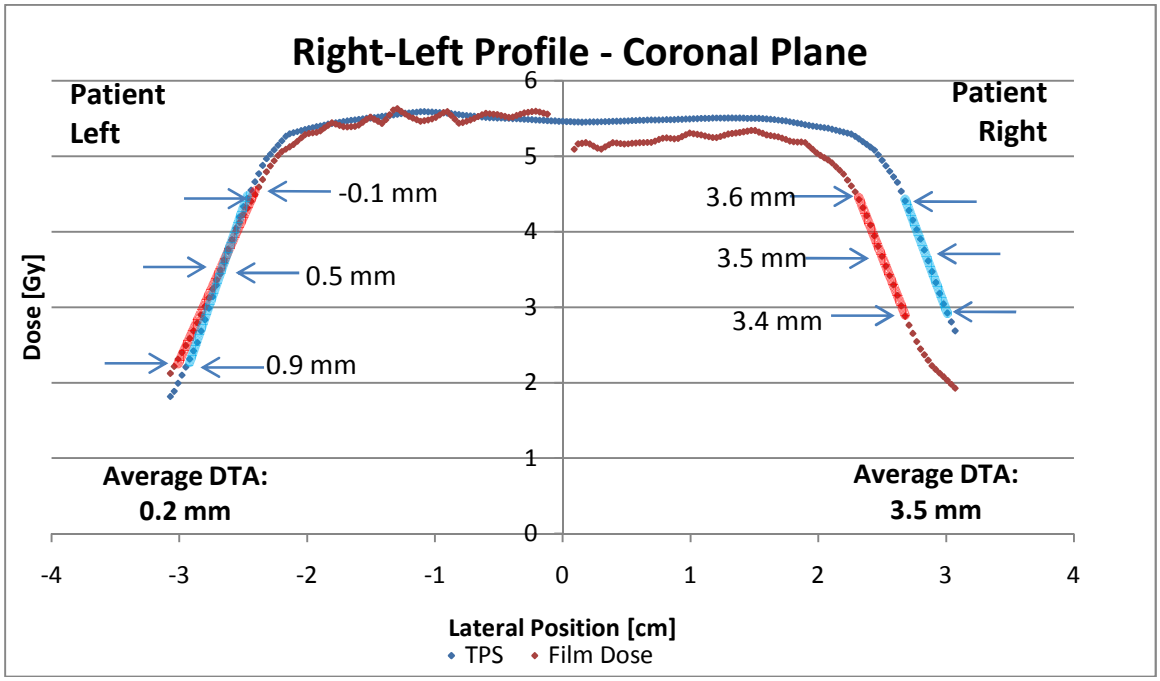

Figure 5.16. Passive scattering trial 3 L-R dose profile DTAs, measured in the coronal plane

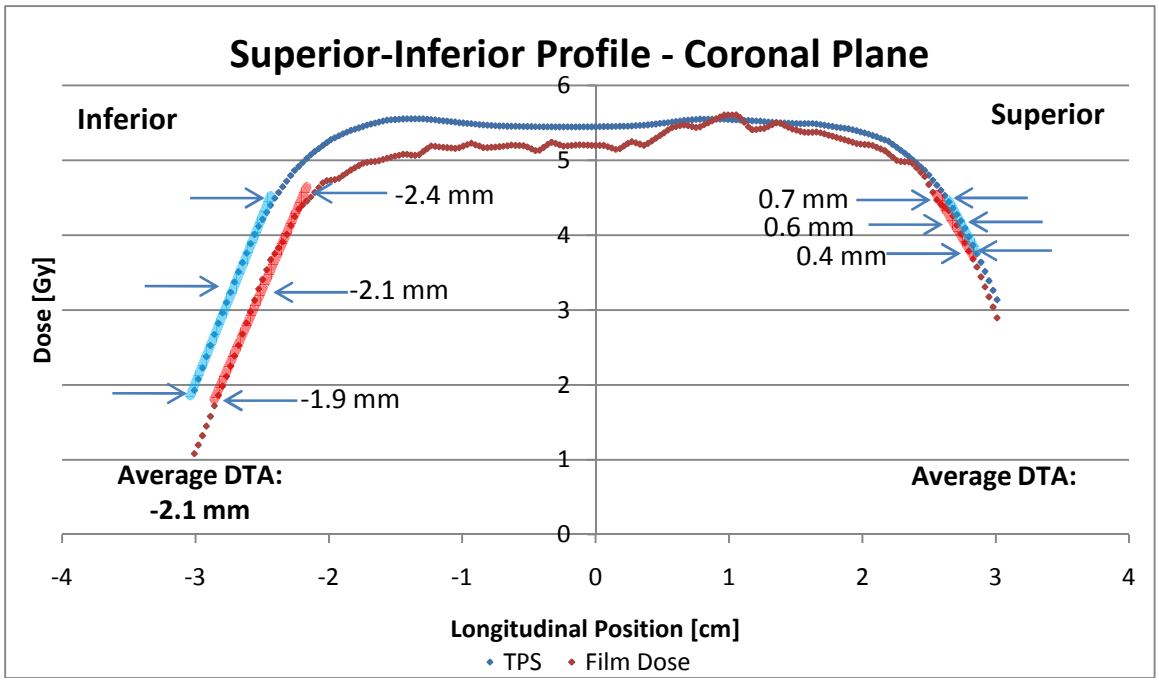

Figure 5.17. Passive scattering trial 3 S-I dose profile DTAs, measured in the coronal plane

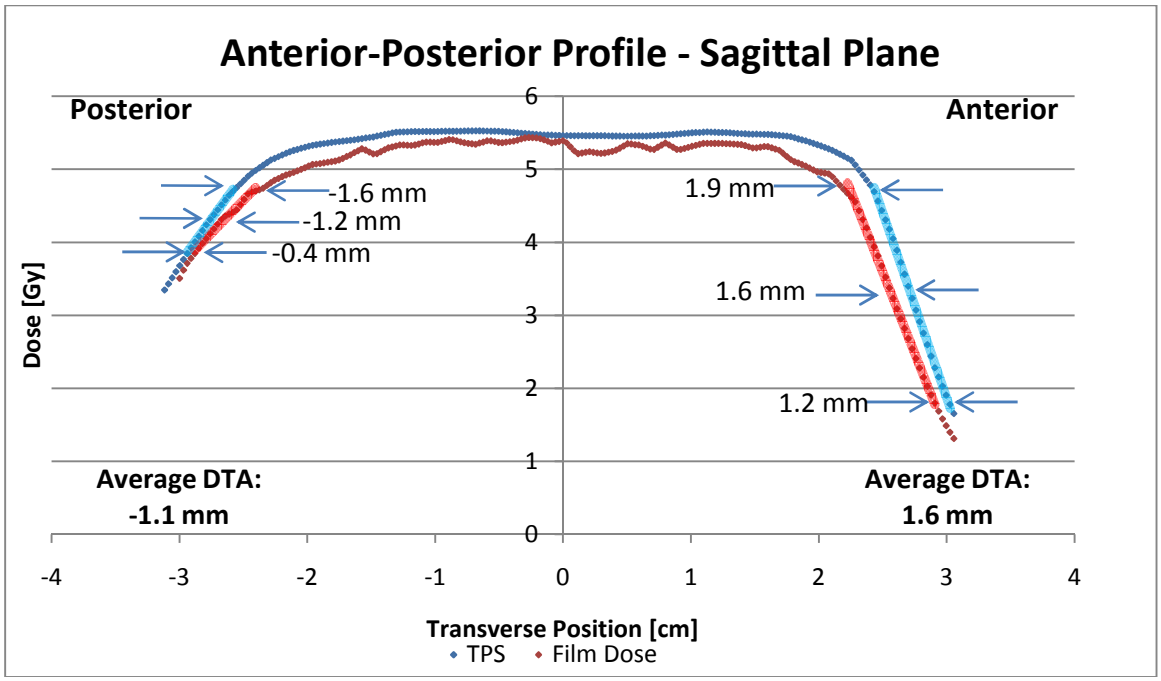

Figure 5.18. Passive scattering trial 3 A-P dose profile DTAs, measured in the sagittal plane

5.2.2 Spot Scanning Plan

5.2.2.1 Trial 1

See Section 3.4.3 for trial 1 results.

5.2.2.2 Trial 2

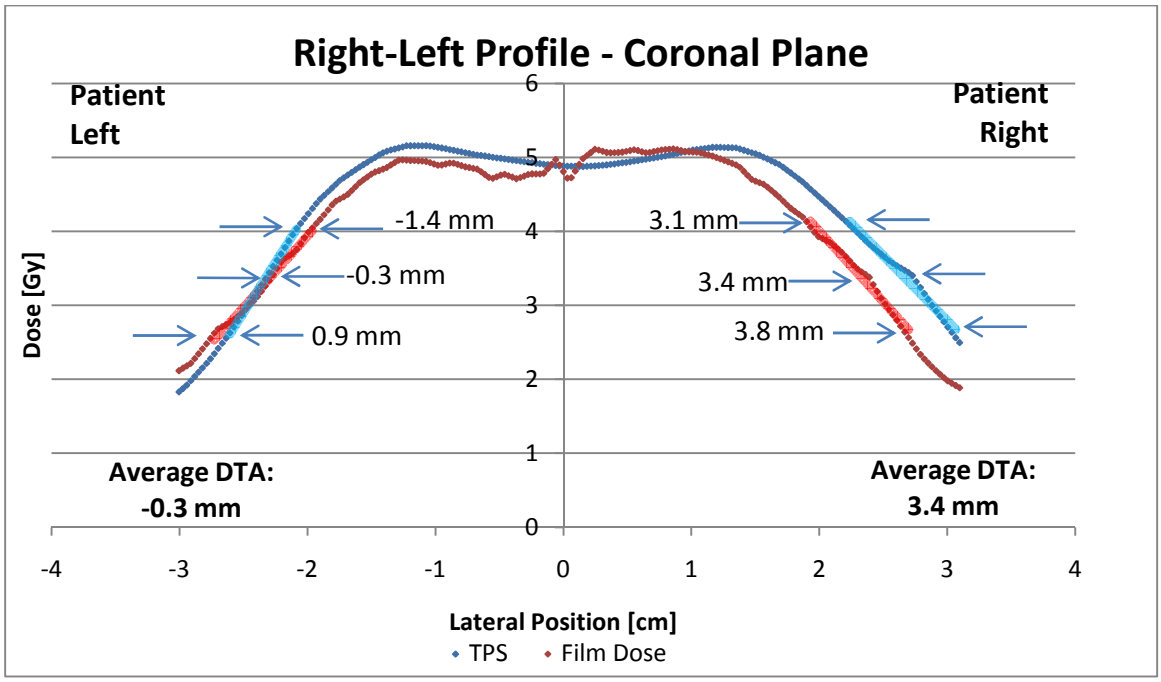

Figure 5.19. Spot scanning trial 2 R-L dose profile DTAs, measured in the coronal plane

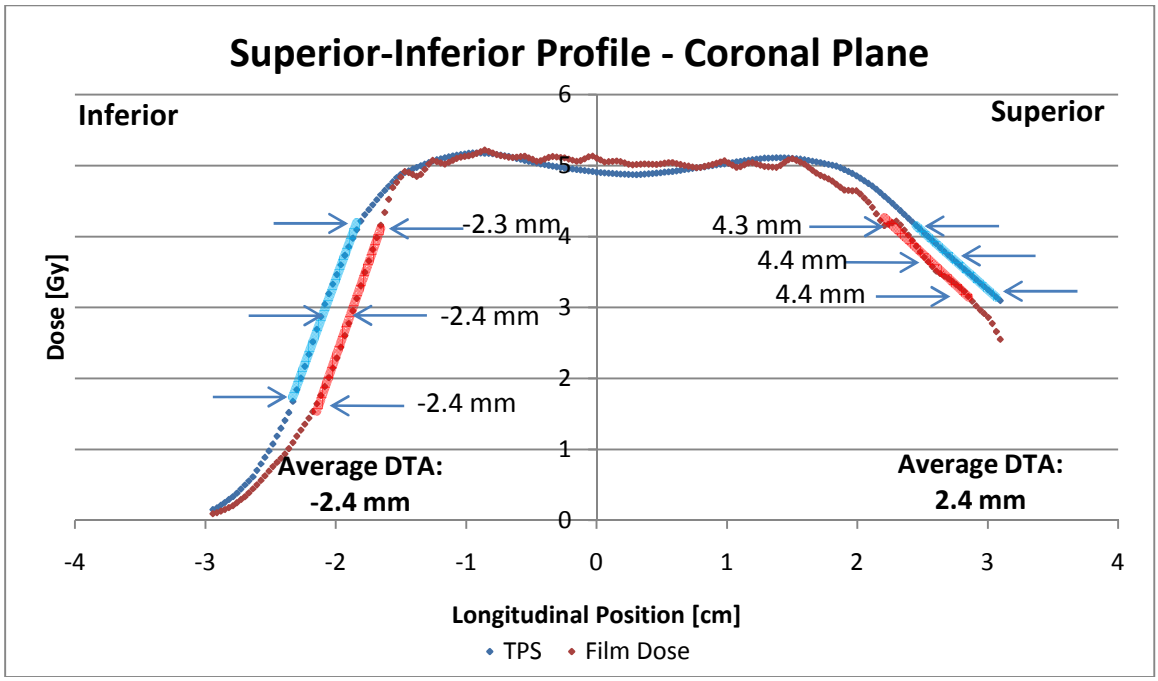

Figure 5.20. Spot scanning trial 2 S-I dose profile DTAs, measured in the coronal plane

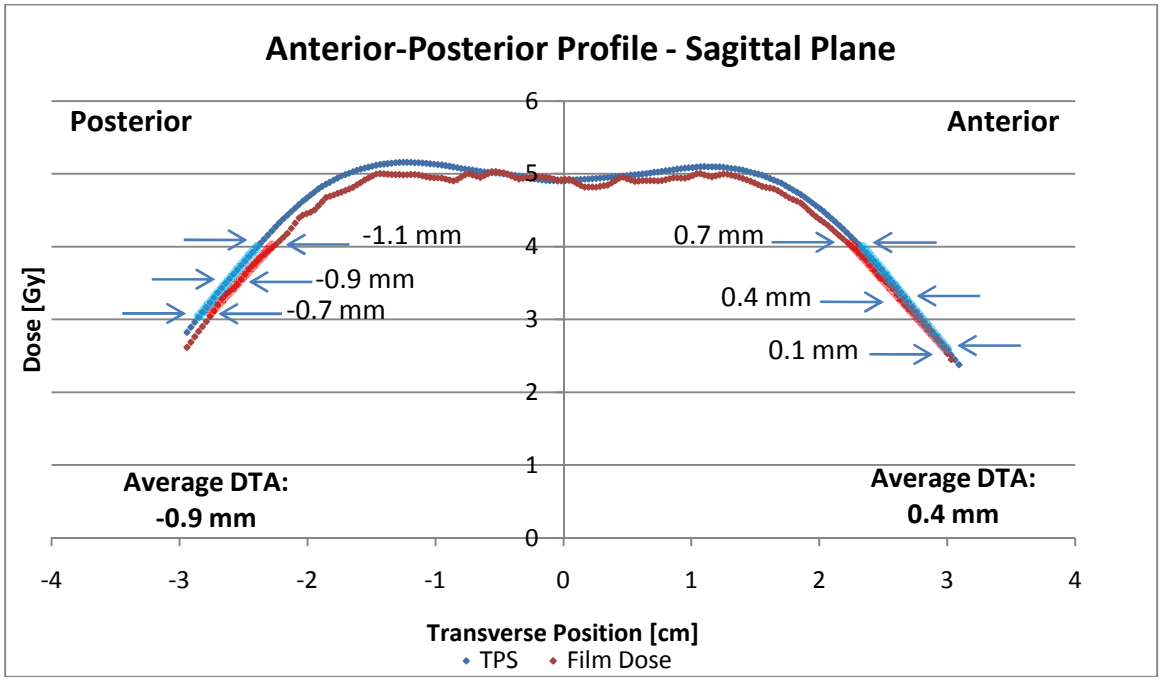

Figure 5.21. Spot scanning trial 2 A-P dose profile DTAs, measured in the sagittal plane

5.2.2.3 Trial 3

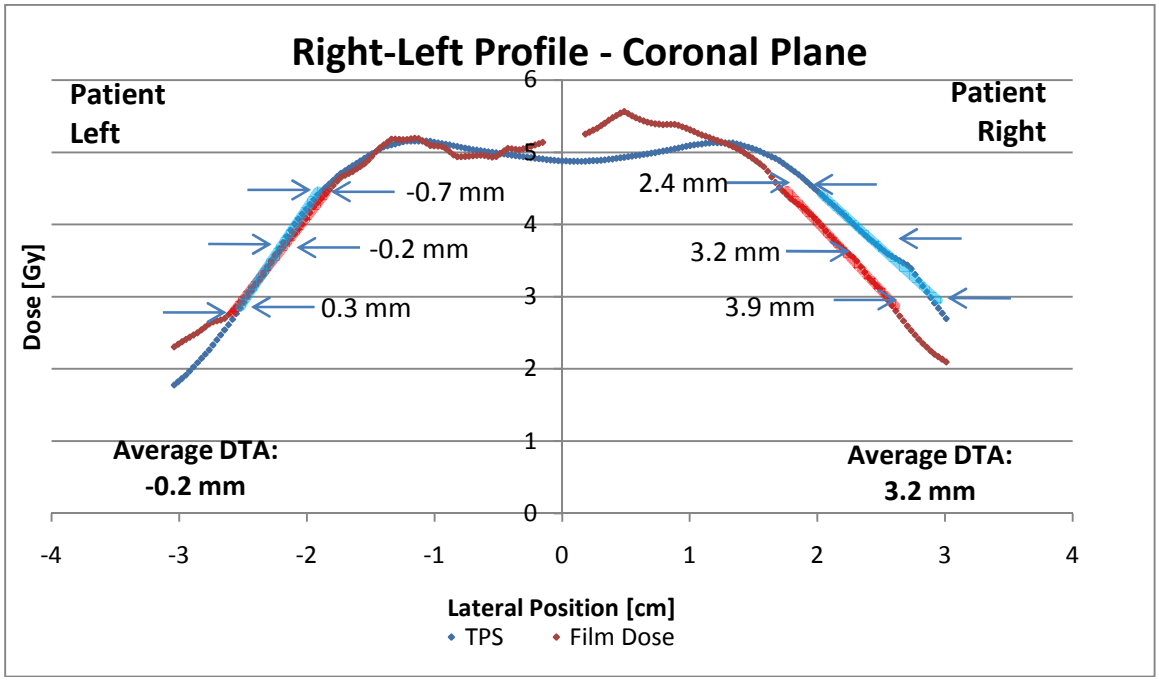

Figure 5.22. Spot scanning trial 3 R-L dose profile DTAs, measured in the coronal plane

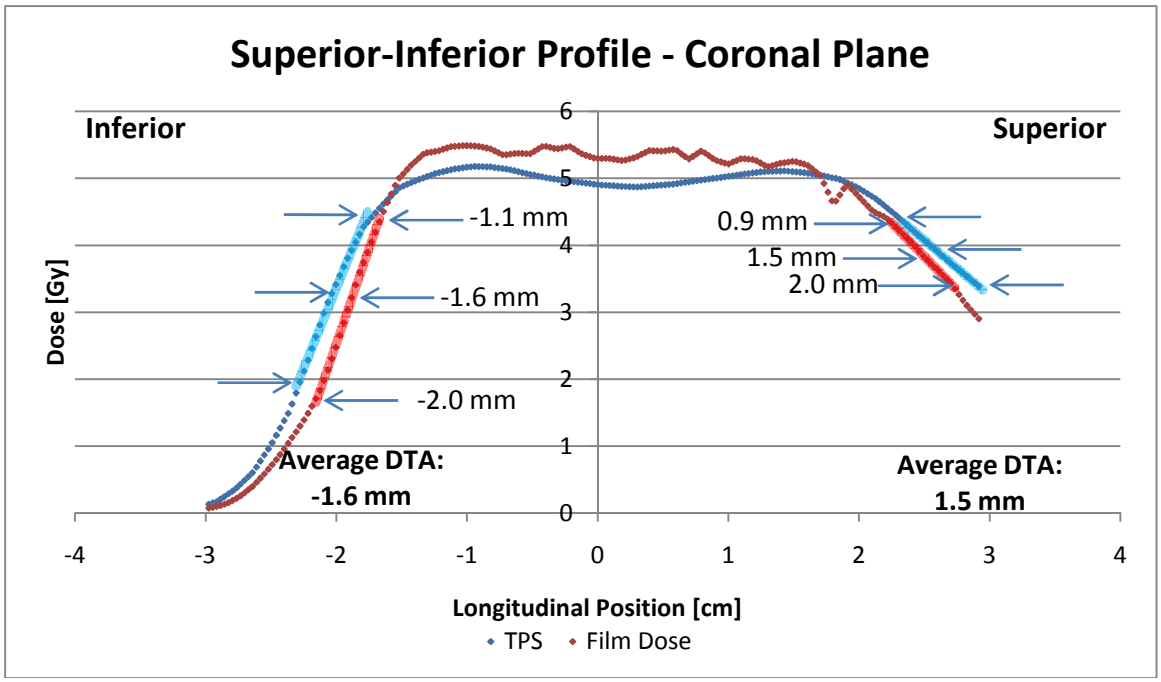

Figure 5.23. Spot scanning trial 3 S-I dose profile DTAs, measured in the coronal plane

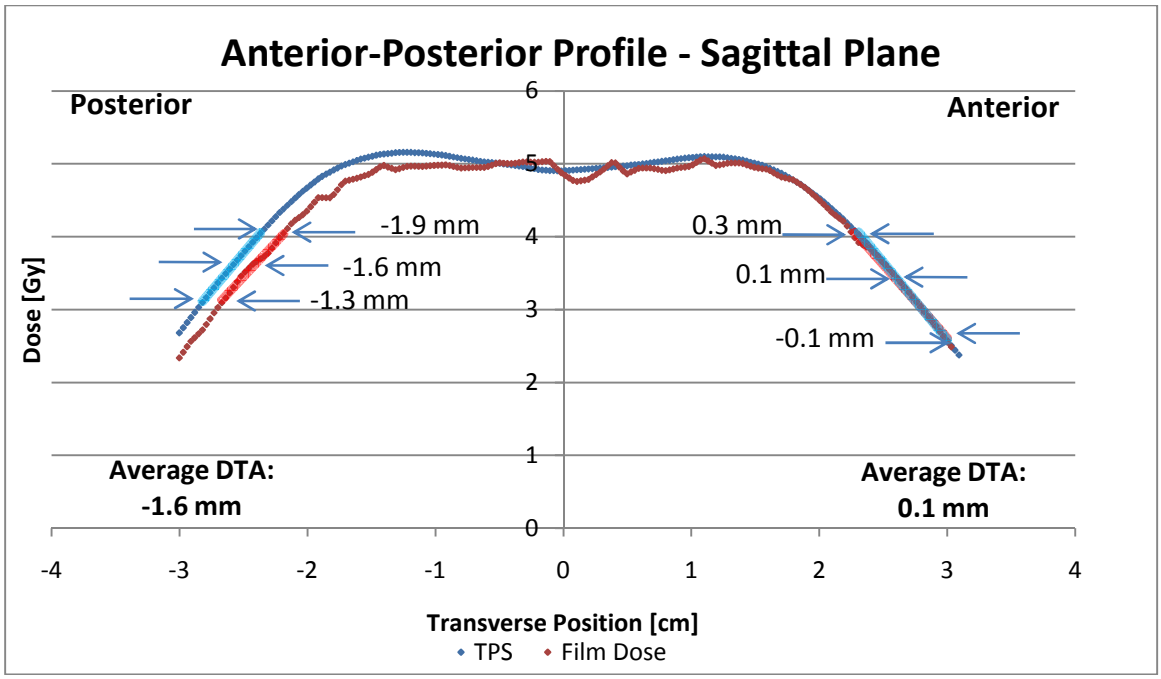

Figure 5.24. Spot scanning trial 3 A-P dose profile DTAs, measured in the sagittal plane

6 References

1. ASTRO. 2010. Statistics: About Radiation Therapy. Fairfax, VA.
2. RPC. 2010. Radiological Physics Center - RPC Website. R. P. Center, editor, Houston, TX.
3. NAPT. 2011. Proton Therapy - The National Association for Proton Therapy (NAPT) Proton Beam Therapy, Protons and Prostate Cancer. National Association for Proton Therapy.
4. QARC. 2010. Quality Assurance Review Center. Providence, RI.
5. Grant, R. 2010. Implementation of an Anthropomorphic Pelvis Phantom for the Evaluation of Proton Therapy Treatment Procedures. In Radiation Physics. University of Texas Health Science Center at Houston, Houston, TX. 103.
6. Blatnica, A. 2011. Modification and Implementation of the RPC Heterogeneous Thorax Phantom for Verification of Proton Therapy Treatment Procedures. In Graduate School of Biomedical Sciences - Medical Physics. University of TX, Houston.
7. Bogdanich, W. 2010. As Technology Surges, Radiation Safeguards Lag. In The New York Times. The New York Times, New York, NY.
8. Bogdanich, W., and K. Rebelo. 2010. They Check the Medical Equipment, but Who Is Checking Up on Them? In The New York Times. The New York Times, New York, NY.
9. ICRU. 2007. 9 QUALITY ASSURANCE. In JOURNAL OF THE ICRU. 135-139.
10. IAEA, P. Andreo, D. T. Burns, K. Hohlfeld, M. S. Huq, T. Kanai, F. Laitano, V. G. Smyth, and S. Vynckier. 2000. Code of Practice for Proton Beams. In Absorbed Dose Determination in External Beam Radiotherapy: An International Code of Practice for Dosimetry Based on Standards of Absorbed Dose to Water. IAEA, Vienna. 181.
11. NCI. 2007. Guidelines for the Use of Proton Radiation Therapy in National Cancer Institute Sponsored Cooperative Group Clinical Trials. National Cancer Institute.

12. RTOG, L. C. Rogers, M. A. Vogelbaum, A. Perry, B. Dean, A. P. Dicker, K. Camphausen, L. Ashby, C. I. Tsien, M. Wang, J. Galvin, H.-M. Lu, and H. A. Shih. 2011. RTOG 0539 - Phase II Trial of Observation for Low-Risk Meningiomas and of Radiotherapy for Intermediate- and High-Risk Meningiomas.
13. Smith, A. R. 2009. Vision 20/20: proton therapy. Med Phys 36:556-568.
14. Wilson, R. R. 1946. Radiological use of fast protons. Radiology 47:487-491.
15. ICRU. 2007. 3 BEAM DELIVERY AND PROPERTIES. In JOURNAL OF THE ICRU. 29-48.
16. ICRU. 1993. 2 ELECTRONIC (COLLISION) STOPPING POWERS FROM BETHE'S THEORY. JOURNAL OF THE ICRU:12.
17. Joiner, M., and A. van der Kogel. 2009. Basic clinical radiobiology. Hodder Arnold ;, London.
18. ICRU. 2007. 1 INTRODUCTION. In JOURNAL OF THE ICRU. 11-20.
19. Paganetti, H., A. Niemierko, M. Ancukiewicz, L. E. Gerweck, M. Goitein, J. S. Loeffler, and H. D. Suit. 2002. Relative biological effectiveness (RBE) values for proton beam therapy. International Journal of Radiation Oncology*Biology*Physics 53:407-421.
20. Weber, D. C., A. J. Lomax, H. Peter Rutz, O. Stadelmann, E. Egger, B. Timmermann, E. S. Pedroni, J. Verwey, R. Miralbell, G. Goitein, and G. The Swiss Proton Users. 2004. Spot-scanning proton radiation therapy for recurrent, residual or untreated intracranial meningiomas. Radiotherapy and Oncology 71:251-258.
21. ICRU. 2007. 2 RADIATION BIOLOGY CONSIDERATIONS. In JOURNAL OF THE ICRU. 21-28.
22. Akagi, T., A. Higashi, H. Tsugami, H. Sakamoto, Y. Masuda, and Y. Hishikawa. 2003. Ridge filter design for proton therapy at Hyogo Ion Beam Medical Center. Physics in Medicine and Biology 48.
23. Smith, A., M. Gillin, M. Bues, X. R. Zhu, K. Suzuki, R. Mohan, S. Woo, A. Lee, R. Komaki, J. Cox, K. Hiramoto, H. Akiyama, T. Ishida, T. Sasaki, and K.

Matsuda. 2009. The M. D. Anderson proton therapy system. Medical Physics 36:4068-4083.

24. Gillin, M. T., N. Sahoo, M. Bues, G. Ciangaru, G. Sawakuchi, F. Poenisch, B. Arjomandy, C. Martin, U. Titt, K. Suzuki, A. R. Smith, and X. R. Zhu. 2009. Commissioning of the discrete spot scanning proton beam delivery system at the University of Texas M.D. Anderson Cancer Center, Proton Therapy Center, Houston. Medical Physics 37:154-163.
25. ICRU. 2007. 4 DOSIMETRY. In JOURNAL OF THE ICRU. 49-81.
26. Zhu, X. R., F. Poenisch, X. Song, J. L. Johnson, G. Ciangaru, M. B. Taylor, M. Lii, C. Martin, B. Arjomandy, A. K. Lee, S. Choi, Q. n. Nguyen, M. T. Gillin, and N. Sahoo. 2011. Patient-Specific Quality Assurance for Prostate Cancer Patients Receiving Spot Scanning Proton Therapy Using Single-Field Uniform Dose. International Journal of Radiation Oncology*Biology*Physics In Press, Corrected Proof.
27. Tew, J., N. McMahon, and T. Orgon-Stamper. 2009. Meningioma. Mayfield Clinic, Cincinnati, OH.
28. Castillo, G. C. 2010. Meningioma, Brain. WebMD LLC.
29. BSF. 2010. Meningiomas - Primary Brain Tumors. Brain Science Foundation, Inc., Wellesley, MA.
30. Gudjonsson, O., E. Blomquist, G. Nyberg, L. Pellettieri, A. Montelius, E. Grusell, C. Dahlgren, U. Isacsson, A. Lailja, and B. Glimelius. 1999. Stereotactic irradiation of skull based meningiomas with high energy protons. Acta Neurochirurgica 141:8.
31. Molineu, A., D. S. Followill, P. A. Balter, W. F. Hanson, M. T. Gillin, M. S. Huq, A. Eisbruch, and G. S. Ibbott. 2005. Design and implementation of an anthropomorphic quality assurance phantom for intensity-modulated radiation therapy for the Radiation Therapy Oncology Group. International Journal of Radiation Oncology*Biology*Physics 63:577-583.
32. Followill, D., D. R. Evans, C. Cherry, A. Molineu, G. Fisher, W. F. Hanson, and G. S. Ibbott. 2007. Design, development, and implementation of the radiological

physics center's pelvis and thorax anthropomorphic quality assurance phantoms. Medical Physics 34:6.

33. Shrimpton, P. C., B. F. Wall, and E. S. Fisher. 1981. The tissue-equivalence of the Alderson Rando anthropomorphic phantom for x-rays of diagnostic qualities. Phys Med Biol 26:7.
34. HAI. 2010. Advanced Markus Chamber Type 34045. Harpell Associates Inc.
35. Moyers, M. F., M. Sardesai, S. Sun, and D. W. Miller. 2009. Ion stopping powers and CT numbers. Medical Dosimetry In Press, Uncorrected Proof.
36. Gottschalk, B. 2004. Passive Beam Spreading in Proton Radiation Therapy. Harvard High Energy Physics Laboratory, Cambridge, MA. 144.
37. Schaffner, B., and E. Pedroni. 1998. The precision of proton range calculations in proton radiotherapy treatment planning: experimental verification of the relation between CT-HU and proton stopping power. Phys Med Biol 43:1579-1592.
38. Sabini, M. G., L. Raffael, M. Bucciolini, G. A. Cirrone, G. Cuttone, S. Lo Nigro, S. Mazzocchi, V. Salamore, and L. M. Valastro. 2002. The use of thermoluminescent detectors for measurement of proton dose distribution. Radiat Prot Dosimetry 101:4.
39. Zullo, J. R., R. J. Kudchadker, X. R. Zhu, N. Sahoo, and M. T. Gillin. 2010. LiF TLD-100 as a Dosimeter in High Energy Proton Beam Therapy--Can It Yield Accurate Results? Medical Dosimetry 35:63-66.
40. Knoll, G. F. 2000. Radiation detection and measurement. Wiley, New York.
41. Kirby, T. H., W. F. Hanson, R. J. Gastorf, C. H. Chu, and R. J. Shalek. 1986. Mailable TLD system for photon and electron therapy beams. International Journal of Radiation Oncology*Biology*Physics 12:261-265.
42. Rosner, B. 2006. Fundamentals of Biostatistics. Thomson-Brooks/Cole, Belmont, CA.
43. Vatnitsky, S. M. 1997. Radiochromic film dosimetry for clinical proton beams. Applied Radiation and Isotopes 48:643-651.
44. ISP. 2009. Gafchromic EBT2 Self-developing Film for Radiotherapy Dosimetry. International Specialty Products, Inc., New Jersey. 17.

45. Soares, C. G. 2006. Radiochromic film dosimetry. Radiation Measurements 41:S100-S116.
46. Zhao, L., and I. J. Das. Gafchromic EBT film dosimetry in proton beams. Phys Med Biol 55:N291-301.
47. Arjomandy, B., N. Sahoo, G. Ciangaru, R. Zhu, X. Song, and M. Gillin. Verification of patient-specific dose distributions in proton therapy using a commercial two-dimensional ion chamber array. Medical Physics 37:5831-5837.
48. Kirby, D., S. Green, H. Palmans, R. Hugtenburg, C. Wojnecki, and D. Parker. 2010. LET dependence of GafChromic films and an ion chamber in low-energy proton dosimetry. Phys Med Biol 55:417-433.

Vita

Paige Alexandra Summers was born in Portland, Oregon on March 4, 1987 to Von and Susan Summers. After graduating Valedictorian of Woodrow Wilson High School in Portland in 2005, Paige continued on to Santa Clara University. In 2009, she received her SCU Bachelor of Science Degree in Physics, with minors in Mathematics and Spanish. In August of 2009 she began her graduate studies at the University of Texas – Houston Graduate School of Biomedical Science, where she is pursuing a Masters in Medical Physics.